Master Thesis

CODEN:LUTMDN/(TMMV-5283)/1-64/2016

Surface topography measurements of thin aluminium foil transferred to FE-simulations

Filip Larsson

2016

DEPARTMENT OF MECHANICAL ENGINEERING

LUND INSTITUTE OF TECHNOLOGY

Abstract

This work is a master thesis preformed by Filip Larsson. The objectives are to measure the aluminium foil used in packaging industry by Tetra Pak. By measuring the surface topography on both sides, the thickness variation will be determined. The measurement results shall then be used in FEM simulations.

The Alicona InfiniteFocus microscope at LTH was chosen to perform the measurements. It is a microscope based on the focus variation technique. The measurements were divided into two rounds; the first round contained measurements on one surface of the aluminium foil while the second round contained rotational measurements.

Several comparisons were made during the work of this thesis. The first comparison was investigating the difference between the two sides of the aluminium foil. This comparison showed that the matt side is coarser then the bright side of the foil. The Sa parameter is 50 % higher for the matt side. The bright side has a clear feature of rolling lines. The rolling lines shows up as clear directions in the gradient images. Surprisingly does the matt side have a main direction as well visible in its gradient image. The direction of the matt side is perpendicular to the direction of the rolling lines on the bright side.

The rotational measurements were never successful so therefore was no true thickness variation achieved. Into the simulation models were two one sided measurements used. The models had a size of 100x100 µm and were set up so they would resemble a little piece of a large tensile test. Three models were used for simulations; they were subjected to tension loading in machine direction (MD), 45 degree direction (45°) and cross direction (CD).

When the correct conditions for the models were achieved all models showed clear localized necks. The strain values were all along the neck well over a 100 % and the maximum was well over 200 %. The neck of the MD model looks like it is following the surface topography of the matt side. The necks in 45° and CD models were probably due to slip band formations and not the topography.

The measurements and their results might not be that reliable. At a maximum were five measurements done on one side, in some case only one per side. This means that the statistical significance is low for the measurement results. That no rotational measurements were successful was due to the hard light conditions. The foil is very reflective and the microscope could not handle the big differences in light during a measurement. During this thesis was a workflow developed that transferred experimental surface topography measurements into a FE-mesh.

Abbreviation

Al – Aluminium

Alumina – Aluminium oxide (Al_2O_3)

CAD – Computer Aided Design

CC – Continuous Casting method

CD – Cross Direction

Cu – Copper

DC – Direct Chill Ingot Casting method

Fe – Iron

FEM – Finite Element Method

LE – Logarithmic strain

MD – Machine Direction

Mg – Magnesium

Mn – Manganese

SEM – Scanning Electron Microscopy

Si – Silicon

XCT – X-ray Computed Tomography

Zn – Zinc

Acknowledgements

To start off with I would like to thank my friends and family. You have all been a big support for me during the last five years leading up to this moment.

I would like to thank Tommy, Olga, Martin, Daniela, Andreas, Viktor and Johan at Tetra Pak. You have all come with valuable input to my work and help me with my progress leading to the results I have achieved.

A special thanks to my supervisors, Ann-Magret and Eskil at Tetra Pak and Mattias at LTH, for the support you have shown. The discussions we have had have been invaluable for this thesis, from how to do measurements and simulations to how to formulate sentences in this report.

Table of Contents

Table of Figures

1 Introduction

This chapter will start with an introduction of Tetra Pak which leads up to the background of the thesis. The problem and purpose will then be described along with the focus and limitations. The chapter will then end with a description of the stakeholders in this thesis.

1.1 Introduction to the company

The idea of Tetra Pak packages were developed in the 1940's by Ruben Rausing. He wanted to develop a new method to store and transport liquid food products, primarily milk, with a better hygiene than the existing solutions at the time. In the early 50's the first package was ready to be launched. It was the tetrahedron shaped package that nowadays is named the Tetra Classic. With increasing popularity the production speed for each packaging machine had to increase. However, this meant that the time for sealing became too short and it leads to leakage problems. The sealing was produced by applying heat on the outside of the packaging material which in turn melts the plastic on the inside. With shorter process time the heat could not penetrate enough to create a stabile seal. This became a big problem threatening the existence of the company.

The problem was solved by introducing aluminium foil on the inside of the packaging material. The aluminium foil allowed the use of induction heating to seal the package. Applying the heat directly on the inside of the paperboard allowed for a faster sealing process.

To broaden the market and make the handling of the packages easier the aseptic packages was developed. For the aseptic packaging, both the packaging material and the content inside of the package must be sterilized. Sterilization means that there are no bacteria that will alter the product in any way. In this development, the aluminium foil showed a positive side effect. The foil acts as a barrier against both oxygen and light. This means that the products nutritional value and taste will not be affected even if it stored at ambient temperature.

1.2 Background to the thesis

Today the thickness of the thin aluminium foil that is used by Tetra Pak in the packaging industry is determined by cutting out a defined area, typically 1 dm^2, of the foil and then to measure the weight of it on an precision scale. The average global thickness is calculated by $t_{avg} = \frac{Mass}{Density \cdot Area}$. The thickness is typically in the order of microns. The existing method has shortcomings as only the average thickness can be determined. A more accurate method for measuring the local thickness and its variation over the foil is wanted.

One technique that been tested was to slit the aluminium foil and measuring the thickness of this cut. However, the aluminium foil was too soft to be able to maintain its structure in the cut. This will give inaccurate thickness measurements. Today the surface topography of the aluminium foil can be measured one side at the time. If it would be possible to measure the foil's surface topography on both sides, and merge these two measurements, it would be possible to determine the local thickness and the thickness variation.

If these measurements later can be imported to FEM software, it is possible to determine the impact the thickness variation and the surface topography have on the strength of the foil.

1.3 Problem and purpose

The objective in this thesis is to find a method to measure the thickness variation and the surface topography, i.e. to quantify the geometrical features, of thin aluminium foil. It is known that the

surfaces on both sides are not smooth, they have a wavy pattern. Today only a rough estimate of the foil's mean thickness is known. It is, however, not known how these wavy surfaces coincide. In some areas the foil can perhaps be extremely thin or thick, and other areas may even be penetrated. These variations need to be studied as it affects the strength of the foil.

It has been studied in previous work that the strength of the foil varies heavily by the direction it is stretched (Käck & Malmberg, 2015). In this thesis it is therefore also of interest to study if this can be explained by the foil's surface topography and the thickness variation. The surface topography measurements of the foil will be imported to Finite Elements simulation software for analysis. The foil will be loaded in three different directions: machine direction (MD), cross direction (CD) and at 45 degrees.

1.4 Focus and limitations

The focus shall be on review existing and novel measuring techniques and see if they could measure the local thickness variation and the surface topographies. A limitation is set to techniques that are available in instruments that might be used in this thesis.

When measurements have been done the focus shall be on find how to transfer the measurements into a FEM model. The FEM model shall then be improved so the simulations resemble physical results as much as possible. The models will not take into consideration the inside structure, i.e. microstructure, of the foils. No grains or voids will be considered nor implemented into the models, only surface topography.

1.5 Stakeholders in the thesis

The author of this thesis will be Filip Larsson, student at Lund University, faculty of engineering. The thesis will be a master thesis of 30 hp (ECTS). Tetra Pak is the issuing part of thesis. They will provide two supervisors: Ann-Magret Asp and Eskil Andreasson. At the university will the Department of Mechanical Engineering provide a supervisor and examiner. Supervisor will be Mattias Svahn at the Division of Machine Element and examiner will be Jinming Zhou at the Division of Production and Materials Engineering.

2 Aluminium

This chapter is fully dedicated to aluminium. It starts out with explaining the production process, how the ore is refined and ends up as a foil with all the steps in between. Further on are aluminium alloys and properties of foil explained. Finally are the foils used in this thesis presented with their similarities and differences.

2.1 Production

Aluminium is a metal that was discovered in the early 19th century. Due to difficulties extracting aluminium, it was not until 1886 by the invention of the Hall-Heroult production process that aluminium started to be mass produced. Production of aluminium consists mostly of sheet, plates and foils, which make up almost half of the total production. Other aluminium products include extrusions and castings. (Woodward, 1994) (The Aluminum Association, Inc., 2007)

2.1.1 From the earth to finished foil

The production process of aluminium foils consist of three different steps, see Figure 1 (The Aluminum Association, Inc., 2007):

1. Aluminium ore - Refined aluminium
2. Refined aluminium - aluminium coils
3. Aluminium coils - aluminium foil

The three different steps are explained below.

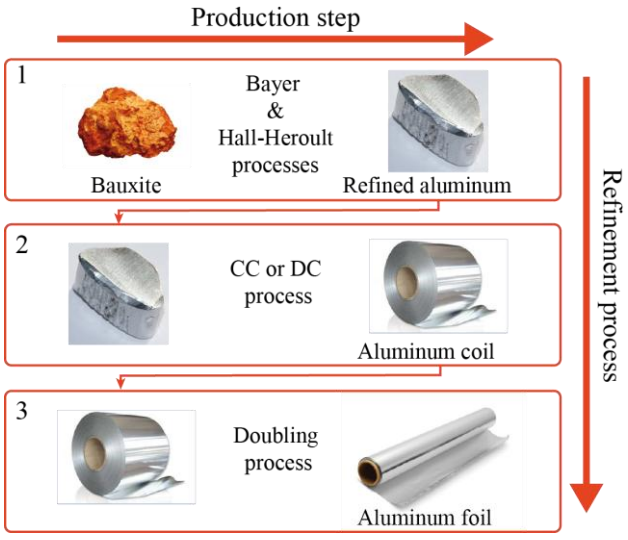

Figure 1. Production process of aluminium foil.

2.1.1.1 Aluminium ore - Refined aluminium

Bauxite is the most common aluminium ore in the world today. To extract the aluminium oxide, also called alumina, from the Bauxite it goes through the Bayer process. The process starts with the

crushed bauxite is put into a bath of caustic soda (sodium hydroxide). At high pressure the alumina dissolves and the undissolved impurities called “red mud” can be removed using filters. The mixture that is left is transferred to a new tank where it is allowed to cool. While cooling down the alumina, it crystallizes and settles to the bottom. It is then removed from the tank and washed so the residual caustic soda will disappear. The final step is heating it so the excess water is removed. The finished alumina is a fine white powder that consists of approximately the same weight of aluminium as oxygen.

The alumina is transformed to pure aluminium by the Hall-Heroult production process. In the process the alumina is dissolved in a molten sodium-aluminium-fluoride salt called cryolite. Electrical current is added making it an electrolysis process. The negatively charged oxygen atoms reacts with the carbon in the positive anode creating carbon monoxide or carbon dioxide, the gases rises out of the bath. The aluminium is heavier than the cryolite which makes it sink to the bottom of the bath. The aluminium is removed and transported to be alloyed and casted. The aluminium produced has a purity of more than 99 %. (The Aluminum Association, Inc., 2007)

2.1.1.2 Refined aluminium - aluminium coils

To get aluminium coils with a strip thickness of around 5 mm from the refined aluminium there are two main methods: the Continuous Casting (CC) method and the Direct Chill Ingot Casting (DC) method. (The Aluminum Association, Inc., 2007)

- Using the CC method, the molten aluminium is allowed to solidify to a continuous strip. The methods for solidify the aluminium are several: roll casters, belt casters and block casters. All these methods make a sheet that will be coiled from the molten aluminium in one operation. That operation typically includes some rolling as well. Figure 2 shows a schematic illustration of a CC production line.

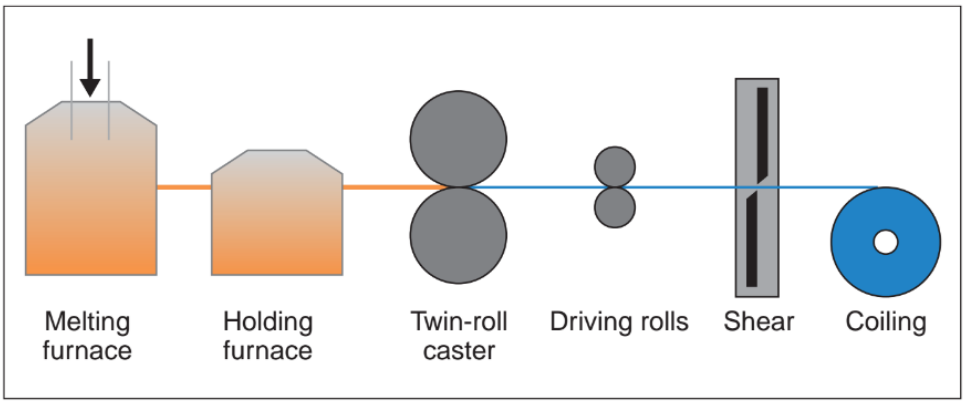

Figure 2. Continuous casting (CC). (Barten, 2002)

- A more common method is the DC method. The DC method consists of two operations to make the coil. The first operation is to make an ingot. The molten aluminium is poured into a shallow mold, but when the sides have solidified creating a shell the bottom starts to move down. This allows the still liquid aluminium inside the solid shell to set as the ingot gets longer when more molten aluminium is poured on top. The final size of an ingot can be as big as 9 meters long, 2.3 meters wide and 0.76 meters thick and weighing about 27 tons. The ingots will then in a second operation be hot rolled through several rolling mills until it requires the requested thickness. Figure 3 shows a schematic illustration over a DC operation.

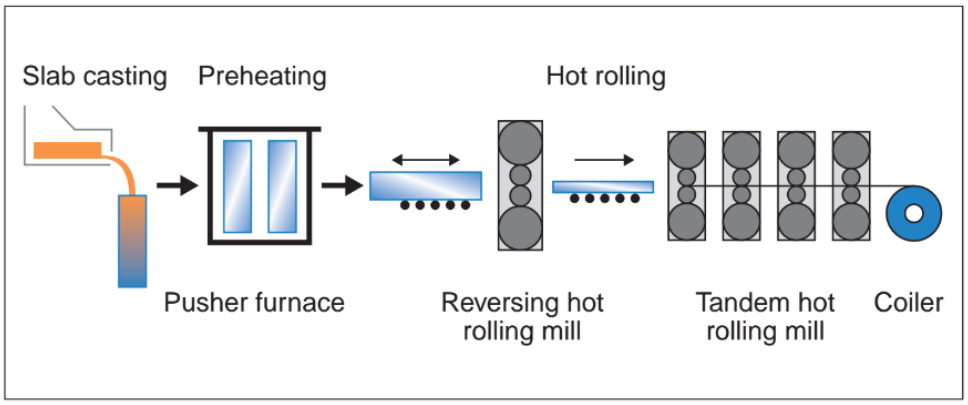

Figure 3. Direct Chill Ingot Casting (DC). (Barten, 2002)

2.1.1.3 Aluminium coils - aluminium foil

It takes many stages of rolling the coil to produce a foil of only a few microns in thickness. The rolling can be done in different kinds of rolling machines. Smaller coils with a weight up to 5 ton can be rolled in reversing roll mills (Figure 4, top). For coils with a weight between 10 and 15 tons mills with the non-reversing single-stand technique is common (Figure 4, middle). Larger rolls and for large production volumes use multi-stand tandem rolling mills (Figure 4, bottom).

The technique used in this third and final step is called cold rolling as the aluminium is worked at a low temperature. During cold rolling not only the global geometry is deformed, the microstructure is changed as well. The grains get elongated and stresses and strains get stored in the material. To restore the original properties of the aluminium and avoid breakage due to high stresses and strains of the foil during the last rolling steps the coils of foil will be annealed. The annealing is typically made twice. The first time is in the middle of the cold rolling process. The second time is after the last rolling, the doubling process.

For the last rolling step, two foils are rolled together in the so called the doubling process (see Figure 5). This procedure gives the characteristic look of one bright and one matt side of the foil. The bright side is the side that is in contact with the rolls. The matt side is in contact with the other foil during this process. The reason for rolling two pieces of foil together is that the desired thickness of the foil could not be met otherwise. To prevent the two foils from fusing together in the doubling process they are rolled with a thin layer of a lubricant in between them.

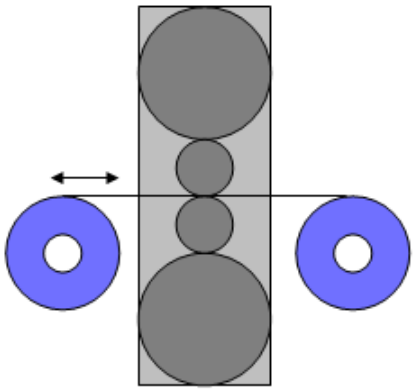

Reversing strip rolling mill

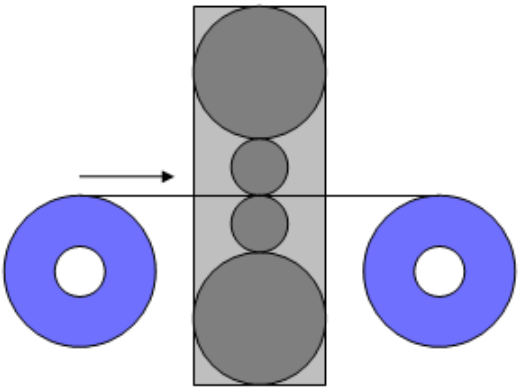

Non-reversing strip rolling mill

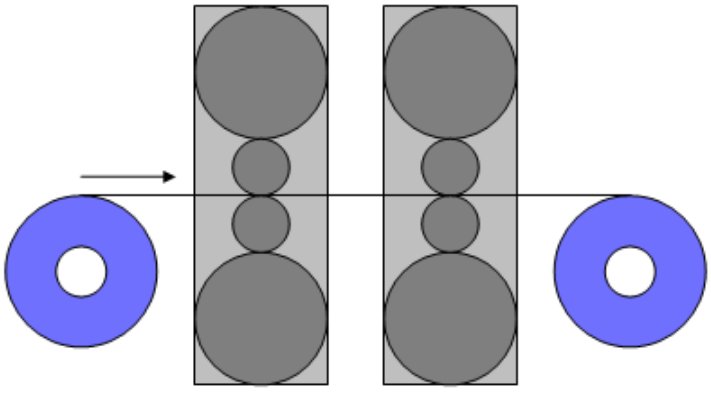

Tandem strip rolling mill

Figure 4. Different types of rolling.

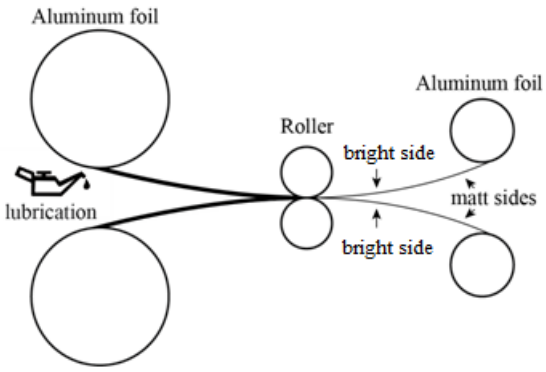

Figure 5. Schematic illustration of the doubling process.

2.1.2 Annealing

When the aluminium is cold rolled the usually ductile aluminium becomes brittle. To restore the original properties the aluminium is annealed. Annealing is a process where the aluminium is heated to a certain temperature and held there for some time. This allows the material to recover from its deformed state and regaining the original characteristics (Callister Jr., 2001).

The annealing has dual purposes. First it is used, as mentioned above, to restore the original properties of the foil. Second to remove lubrication residues from the coil of aluminium foil. To restore the original properties is a fairly quick process but to remove the lubrication residues takes longer time. This is because the lubrication needs to seep from the coils center to the edge to be able to evaporate.

During the annealing process there are three steps. They will be explained below. In Figure 6 are the features of the annealing process visualized.

2.1.2.1 Recovery

The first step in the annealing process is the recovery. In this stage the dislocations in the material is moving to the grain boundaries and dissolve. This movement relieves some of the stored strain energy and is a result of the increased atomic diffusion due to the elevated temperature.

2.1.2.2 Recrystallization

After the recovery stage there is still relatively high strain energy in the grains. During recrystallization, the old grains get transformed to newly formed grains which are strain and stress free. The new grains start out as small nuclei and with short-range diffusion they take atoms from the old deformed grains, finally ending up replacing them completely. The new grains have the same properties of the pre-cold rolled grains.

Recrystallization is a diffusion driven process, and depends on both temperature and time. Time influence the degree of recrystallization, longer time allows creation of more new grains.

2.1.2.3 Grain growth

The third and final step during the annealing is the grain growth. It takes over after the recrystallization when all the old deformed grains have been replaced by new grains. However, the

process of atomic movement between grains continues. This result in smaller grains dissolves and its atoms join other grains, creating larger grains than earlier.

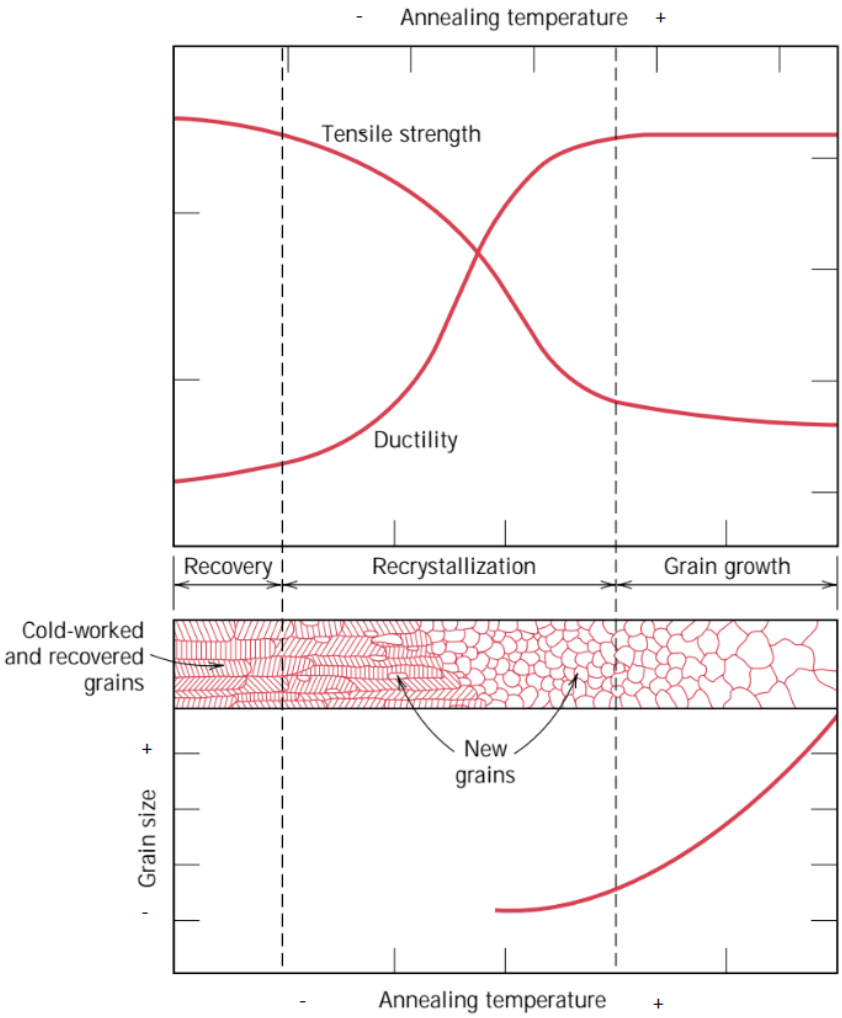

Figure 6. The annealing process with its three parts. (Callister Jr., 2001)

2.2 Alloys

Pure aluminium has not very high mechanical strength, which limits its range of different applications. To get higher strength and other characteristics to make it possible to use in a wider range of applications, other materials are mixed in, the aluminium is alloyed. The most common alloying elements for aluminium alloys are silicon (Si), magnesium (Mg), manganese (Mn), copper (Cu) and zinc (Zn). Some iron (Fe) is found in all aluminium alloys and it originates from the production process, but Iron can also be added as an alloying metal. (European Aluminium Association, Støren, & Skanaluminium, 1994)

Aluminium alloys are usually classified after their major alloying element. Table 1 shows the classification along with some properties of each series.

Table 1. The different Al alloy series with their major alloying elements and comments (The Aluminum Association, Inc., 2007)

Alloy series	Major alloying element	Comments
AA1xxx	Aluminium of 99 % or higher purity.	• Excellent corrosion resistance • Thermal and electrical conductivity.
AA2xxx	Cu	• Substantially strength after heat treatment
AA3xxx	Mn	• Generally non-heat treatable
AA4xxx	Si	• Generally non-heat treatable
AA5xxx	Mg	• Generally non-heat treatable
AA6xxx	Si & Mg (creating Mg_2Si)	• Heat treatable
AA7xxx	Zn	• Heat treatable • Very high strength
AA8xxx	Various other compounds.	

Tetra Pak uses Al-foils from the AA8xxx-series with the most prominent alloying materials being Iron and Silicon. Iron has high solubility in molten Al but only 0.05 % in solid Al (Bengtsson, o.a., 2014). This result in much of the Fe gets concentrated at the grain boundaries during solidification. With higher Fe content more grain boundaries appear and the grains become smaller. The soluble Fe and Si atoms hinder big movements and concentrations of dislocations which make the material stronger. Smaller grains allow more flexibility and movement in between the grains, which results in higher ductility. (Mishina, 2016)

2.3 Production induced properties and defects of the Al-foil

During the production when the material is formed certain properties and defects occur. The alloying materials should theoretically spread out evenly in the aluminium lattice but that is not always the case. If the alloying materials are concentrated, grains that are harder than the other can form. Those grains can puncture and make holes in the other foil during the doubling process. These defects are so called pinholes. Pinholes are more common the thinner the foil is and it influences the strength of the foil. Pinholes in the foil can act as start points for cracks. Also, holes in the foil compromise the oxygen and light barrier in the packaging material.

The annealing process is used to replace the elongated grains that have formed during the rolling with new round ones. The process is also used to remove the lubrication that is used in the rolling process. However, as the foil is rolled up as large cylinders, it is very hard to remove exactly all

lubrication. Potential leftovers can possible influence the measurements that will be performed on the surface of the aluminium foil.

As mentioned above the aluminium foil gets a bright and a matt side in the final rolling steps during production. The matt side originates from being in contact with the other foil during the doubling process and the bright side form being in contact with the work rollers. Therefore, before the doubling process are both sides of foil bright. The production of the work rollers results in a striped surface. This stripes make an imprint of the foil when worked, the foil get so called rolling lines. However, when doubled the matt side is created as mentioned above. This changes the surface topography to a more arbitrary topography from the clear directional topography with the lines. In Figure 7 are the two images, one of a bright side and one of a matt side to visualize the differences.

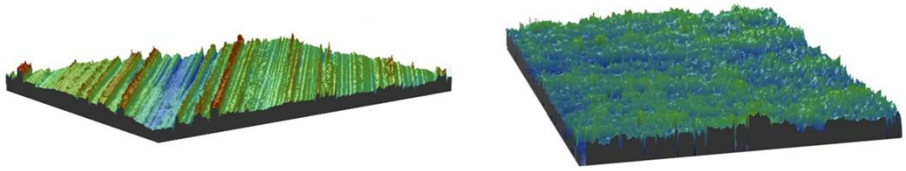

Figure 7. The bright (left) and the matt (right) surface of the foil. (Bengtsson, o.a., 2014)

2.4 The aluminium foil

In this thesis five different Al-foils have been measured to establish different relations between them. Table 2 contains the foils used in this thesis and some information about each.

Table 2. Foils used in this thesis

Foil	Manufacturer	Alloy	Thickness [µm]
#1	Manufacturer A	AA8079	9,0
#2	Manufacturer A	AA8079	6,3
#3	Manufacturer B	AA8011	9,0
#4	Manufacturer B	AA8011	6,3
#5	Manufacturer C	AA8079	6,3

Two different alloys are studied. Both alloys have the same major alloying elements, namely Iron and Silicon, but in different proportions. The reason for Manufacturer B to use a different alloy than the other manufacturers is that their production uses another technique. Manufacturers using the DC technique make foils with the AA8079 alloy and manufacturers with the CC technique use alloy AA8011. Despite the different alloys and production techniques, foils with the same thickness should have similar mechanical properties.

3 Experimental techniques for measuring 3D surfaces

One objective of this master thesis is to determine the surface topography of aluminium foil. There are several measuring methods that can be used to achieve this. In this report, two groups of methods are described.

The 3D-surface methods can only determine the surface topography of the sample, whereas 3D-voulme methods create a 3D model of the whole specimen. They measure the inside as well as the surfaces of the specimen. In this chapter are some of the methods from the two categories explained.

3.1 3D-surface measurement methods

To measure the surface texture there are many different methods. In the standard ISO 25 178-6:2010 (SIS, Swedish Standards Institute, 2010) a total of 19 methods, sorted in three categories, are defined and explained, see Figure 8. The three categories are line profiling, areal topography and area integration.

1. Line profiling measures the surface topography along a line and produces a two dimensional graph of the height as a function of the distance, z(x), or angle, z(θ).
2. Areal topography measures the surface topography over an area resulting in an image of the surface roughness. The height can be expressed as a function of the position, z(x,y).
3. Area integration measures an area and produces a numerical value depending on the surface texture.

Methods that have the possibility to perform both line profiling and areal topography have often originated from a line profiling method that has been remodeled to do several measurements at once and stitch them together so a topography is created.

With the objective in this thesis to measure the surface topography of both sides in one measurement the areal-topography method is the most suitable. Out of the 19 standardized methods there are 13 methods capable of doing surface topography measurements. There are advantages and disadvantages with every method but there will not be a review of them all in this thesis. The focus will be on those methods that are present in instruments that might be used in this thesis: the focus variation method and the angle resolved scanning electron microscopy method.

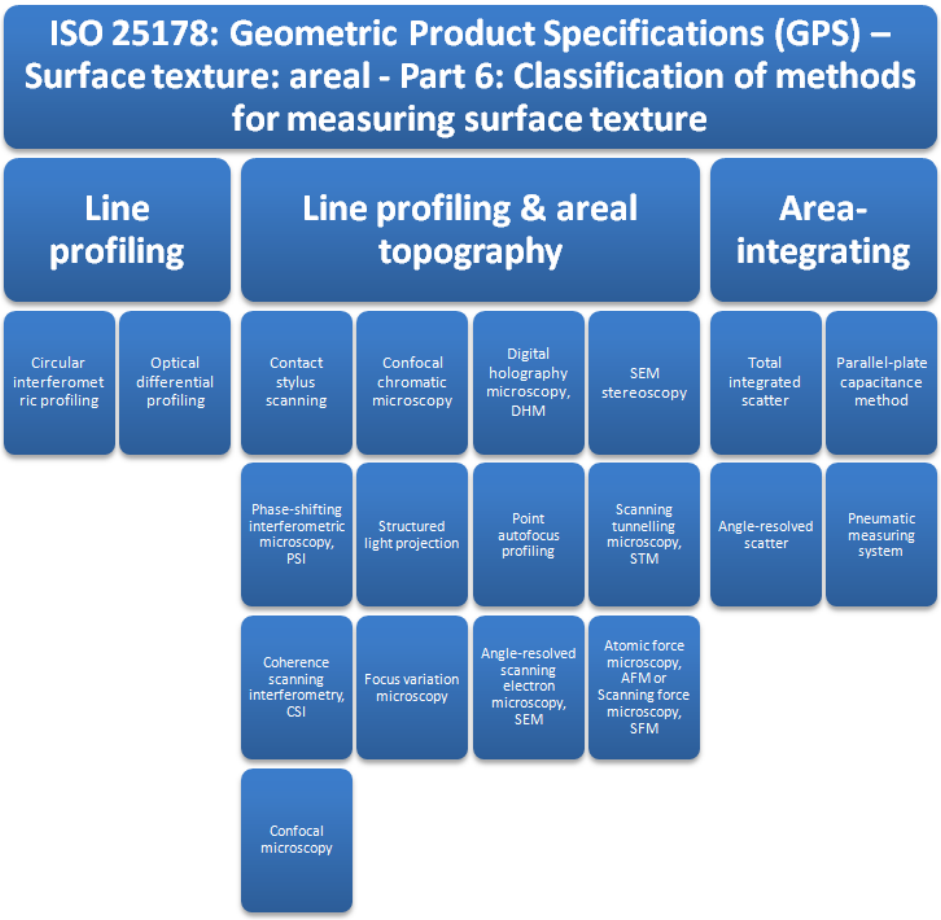

Figure 8. The 19 different techniques standardized in ISO 25178-6

3.1.1 Focus Variation Microscopy

The Focus Variation (Reinhard Danzl, 2011) microscopy method is defined in the ISO 25178-6 standard as:

> *Surface topography measurement method whereby the sharpness of the surface image (or another property of the reflected light at optimum focus) in an optical microscope is used to determine the surface height at each position along the surface. (SIS, Swedish Standards Institute, 2010)*

What it means is that the short focus range of the microscope is utilized to find on which height each point of the surface have. An upper and a lower search limit are set and the microscope conducts a search in between. When all search levels are scanned the images are compared and each point is assigned a height at which level they are in focus. This creates a topography map of the measured surface. How a microscope with focus variation is typically set up is shown in Figure 9.

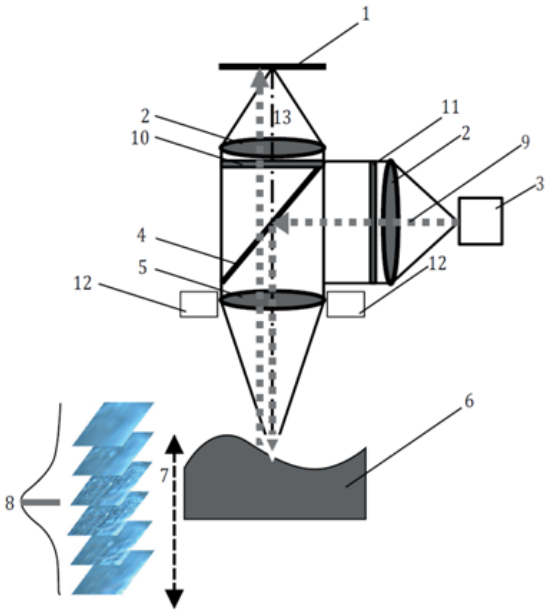

1. Array detector
2. Optical components
3. White light source
4. Illumination beam splitter
5. Objective
6. Specimen
7. Vertical scan
8. Focus information curve with maximum position
9. Light beam (…)
10. Analyzer
11. Polarizer
12. Ring light
13. Optical axis (.-.-.)

Figure 9. Typical setup for instrument based on focus variation.

Advantages with the focus variation method are several. First is that it is a non-contact method, this means that the sample does not get damaged or altered by a probe. With no part in contact with the sample, there is less wear and tear on the microscopes parts which means lower maintenance of the instrument. With focus variation you are not limited to the light emitted by the microscope. If the light from the microscope is regarded insufficient it is possible to have an extra light source that helps illuminating the sample. That so enough light is reflected back into the objective to give a clear image. This makes it possible to measure steeper flanks than in other microscopy techniques. By using white light the whole visible color spectrum is utilized so the light reflected back into the microscope represents the true colors of the sample.

A problem with the focus variation method is that it requires an opaque sample. If the sample is transparent, the microscope can have trouble finding the surface and the corresponding height position.

3.1.1.1 Alicona InfiniteFocus

An instrument that utilizes the focus variation technique is the Alicona InfiniteFocus microscope (Alicona, 2016). It has six different objective lenses with a magnification in the range from 2.5x to 100x times. With the 100x objective the vertical resolution is as little as 10 nm while the lateral resolution is 440 nm and the minimum measurable roughness (Sa) is 0.015µm. The measurement is visualized as a 3D model with possibilities to measure the profile form, profile roughness (Ra,Rq,Rz etc.), surface texture (Sa,Sq,Sz etc.) and much more. The result can also be exported as a 3D data set in several different file formats (e.g. STL). The Alicona microscope also offers multiple options for lighting up the sample. These options are regular and polarized white light and can be combined with a secondary light source in form of a ring light.

The microscope seen in Figure 10 is located at the Department of Production and Materials Engineering at Lund University. This particular microscope has accessory and software that allow the sample to rotate during the measurement. This makes it possible to measure both sides of the Al-foil in one measurement.

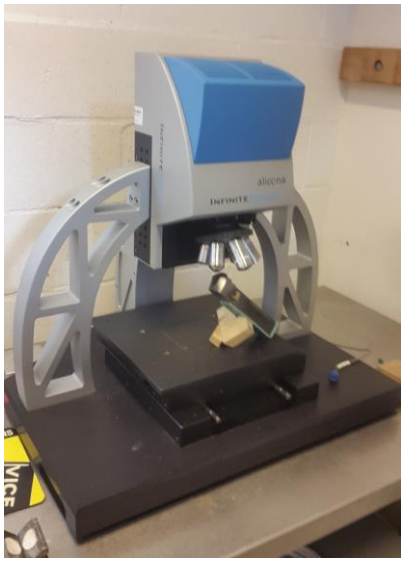

Figure 10. The Alicona InfiniteFocus at LTH.

3.1.2 Angle Resolved Scanning Electron Microscopy, SEM

All SEM microscopes use an electron beam to create an image of the specimen and not visible light as regular microscopes. The electron beam is created with high voltage in the top of the microscope and is then focused down towards a specific point on the specimen. The electrons in the electron beam are called primary electrons. The interaction between the primary electrons and the specimen results in electrons of the atoms of the specimen getting knocked out of the atom. The knocked out electrons is called secondary electrons. Some of the primary electrons gets reflected back from the specimen and are called backscattered electrons. The secondary electrons are detected and the amount registered defines how bright the measured spot will be in the result image.

With the use of electrons there is a need for a vacuum chamber for the measurements to take place, this so the electron will not interact with the ambient air. This makes the microscope more complex to handle and it will also require more maintenance than a regular microscope with white light.

Angle resolved SEM creates a 3D image by combining gradients from different measuring points on the surface. The gradients are calculated by the intensity of the directions of the backscattering electrons.

3.1.2.1 Hitachi TM3030 Tabletop microscope

This microscope uses a backscattered electron detector to create a 3D image which implies the use of the angle resolved SEM technology. It has magnification options from 15x up to a staggering 30 000x. With special software it is possible to do 3D measurements and extract surface parameters from the measurements. However, in contrast to the Alicona there is no rotational option so only one side of the foil can be measured in one measurement.

This is the SEM microscope being installed at Tetra Pak during the implementation of this thesis. Due to some installation and start up problems this microscope never became available during the thesis.

3.2 3D-volume measurement methods

To be able to measure the whole volume of a specimen and not only the surface the method must use something that can penetrate the material of the specimen. As aluminium foil is not being a clear material, visible light is therefore ruled out. Methods possible to fulfill this requirement for aluminium foil must be using some other source for data collection, for example x-rays.

3.2.1 X-ray Computed Tomography, XCT

X-ray computed tomography uses x-rays to perform the measurements. X-rays will penetrate the material and create a 3D image of the specimen.

A XCT instrument consists of mainly three parts: an x-ray source, an x-ray detector and a rotation table in between for the specimen to sit on. The source produces and sends out x-rays towards the sample. The attenuation of the x-rays through the sample gets recorded by the detection plate and creates a regular x-ray image. With measurements performed at many different angles the resulting images can be reconstructed into a 3D model of the sample with an attenuation coefficient for each part.

There are two main techniques for the reconstruction process, the algebraic and the analytical technique. The algebraic consists of a linear equation system from which the different attenuation coefficients should be solved. The principal of the analytical method is to back project the recorded intensities with a Fourier transform. With the sample rotating a filter is needed for the back projection which gives the method its name, filtered back projection reconstruction. The analytical method is the faster reconstruction process. However, it requires a complete scan around the object, which is very time consuming. The back projection algorithm must be adjusted for the x-ray source used. Medical and industrial scanners often use an x-ray source that is producing a cone beam of x-rays while synchrotrons create x-rays that are parallel to each other. (Buffiere, Maire, Adrien, Masse, & Boller, 2010)

The resolution with XCT have until a few years ago only been in the micro scale. Then techniques for nano scale measurements were developed for both industrial scanners and synchrotrons. However, that come with a much longer acquisition time for each measurement. For example have a spatial resolution of just 12 nm been achieved (Maire & Withers, 2013). However, this fine resolutions have been achieved with low energy x-rays and they have more difficulties to penetrate harder material such as metals.

An advantage with XRCT is that it is a non-contact method just like the methods above and that it is possible to see the inside structure of the sample. However, the use of x-rays makes the technique so much more complex. This means it is harder to handle and it is likely to need more maintenance than a regular white light microscope.

3.2.1.1 Zeiss Xradia 520 Versa

The tomograph located at the division of Solid Mechanics at Lund University is of the brand and model Zeiss Xradia 520 Versa. The x-ray source is what they call a sealed transmission x-ray tube and it works at a voltage of 30 to 160 kV. An x-ray tube creates x-rays by accelerating electrons between a cathode and an anode. Upon impact the electrons reacts with the anode material that is usually tungsten, W, to create x-rays by bremsstrahlung (Bruker AXS, 2006).The resolution of the Xradia 520 is as its best around 700 nm. That resolution is probably too low for measuring the topography of the aluminium foil.

4 Measurements of surface characteristics

In this chapter will it first be described how the measurements have been done. There will be procedures for both one sided and rotational measurements. Then are the measurements that been performed explained. Finally are there explanations of which parameters that can be used to characterize the measurements.

4.1 Procedure for measurements

All measurements have been done on the Alicona InfiniteFocus microscope at LTH.

The measurements in this thesis have been divided into two different rounds. In the first round only one surface will be measured at a time. This is to get familiarized with the microscope used and to learn how handle it. In the second round rotational measurements will take place so both sides can be measured relative to each other.

4.1.1 One sided measurements

During these measurements only on side is measured at a time. This means that the foil will be static during the measurements.

4.1.1.1 Preparations

Before any sample can be put under the microscope it needs some preparations. The sheets of Al-foil where separated carefully so no wrinkles would be created. When separated, the sheets where cut with scissors to appropriate size, approximately ten by ten centimeters. Two samples where cut so measurements could be done on both sides without the need to redo the preparations when one side had been measured. The two samples were put on a thick piece of plastic that acted as support of the foil during the measurements.

The aluminium foil needed to be washed with ethanol before any measurements could be performed. This operation was done to remove much of the left over lubrication from the production and other impurities on the surface, such as fat from fingerprints etc. Ethanol was used excessively so as much as possible of the impurities would be removed. The ethanol was applied on the top side but also in between the foil and the plastic support, this created a suction effect and gave extra stability during the measurements. The ethanol did flow back and forward over the foil before it was allowed to run off, the excess ethanol still left on the aluminium foil was allowed to evaporate before the measurements were started.

4.1.1.2 Measurements

As described in Section 3.1.1 focus variation works by taking images at various heights. To perform a measurement with the Alicona InfiniteFocus a few parameter must be set. First when the sample is put under the microscope the surface must be found, i.e. to find the correct height of which the sample is in focus. The light intensity must also be set correctly for the given sample. The light setting for very reflective surfaces is tricky as a lot of light is reflected back into the objective and consequently the detection sensor. The brightness of the main light and the ring light of the microscope can be set individually and a polarization filter can be used as well on both light sources.

When the surface is found with adequate light settings, a vertical scan range appropriate for the sample must be set. The range must be large enough to cover the complete sample. This ensures that all parts of the sample will be in focus once. Flat placement of the specimen is therefore preferable over a tilted, since a smaller scan range results in shorter scanning time. When a good range is set only the resolution settings needs to be chosen before the measurement could start.

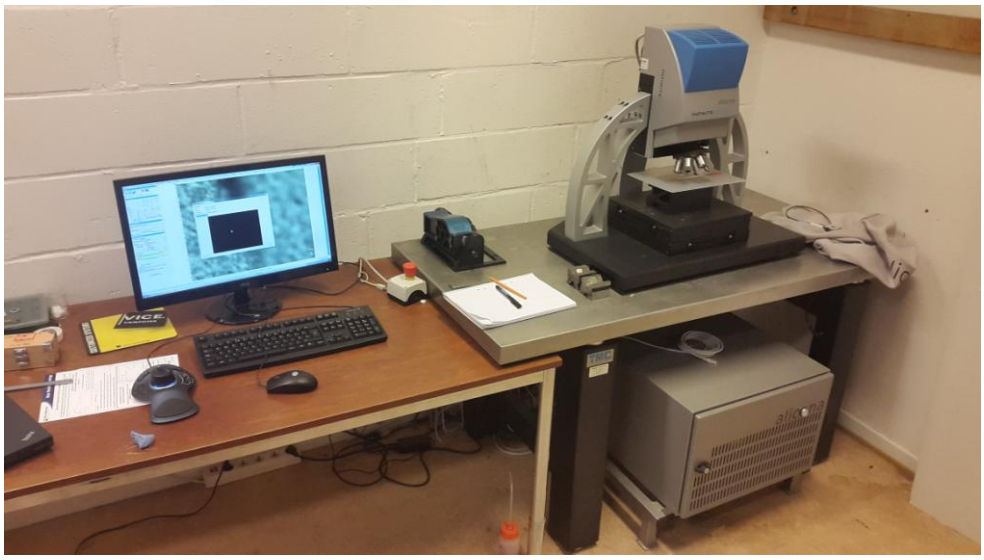

Figure 11. The Alicona InfiniteFocus instrument at LTH during a measurement.

4.1.1.3 Post-processing the measurement results

Some post-processing of the measurements is needed before some results can be produced. The edges in some of the measurements can have a missing part or an outlier, i.e. a measuring point with improbable results compared with the measuring points surrounding it. Missing parts and outliers will be removed, so that these do not affect the surface parameters.

Before results are extracted the measured surface is also corrected with an F-operator, see section 4.3.1. This to make sure the coordinate system of the measured surface will coincide with the global coordinate system as reference plane for calculating different result parameters will be based on the global coordinate system.

4.1.2 Rotational measurements

During these measurements the Al-foil specimen will be rotated so both sides can be measured in one measurement. This so the surface topographies of both sides can be related to each other and create a thickness variation of the foil.

4.1.2.1 Preparations

To do rotational measurements a rig is needed so both sides of the foil can be exposed to the instrument. Therefore have a special holder for the foil been designed. The designed holder is a stick that can be placed in the rotational part of the instrument with a frame at the other end upon which the foil could be placed. This design meant that the measurement would be done around the frame. In a later design only half of the frame was implemented leading to a free edge of the foil

would be placed in the rotational axis. Both designs of foil holders are presented in Figure 12. The size of the foil holder and therefore later the piece of Al-foil is very small. This is to fit under the microscope while rotating without hitting the objective and to have a smaller scan range. A smaller scan range leads to a shorter measure time.

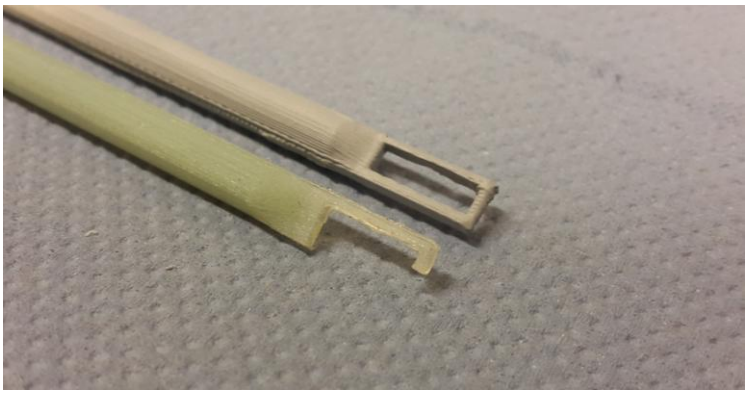

Figure 12. Foil holders used for rotational measurements.

The foil was separated and cut into a piece that would fit on the foil holder. A small amount of glue was put on the holder and on top of it the small piece of foil. When the glue has set the Al-foil is washed with ethanol. Then was the foil holder placed in the rotational accessory of the instrument.

4.1.2.2 Measurements

As for one sided measurements a scanning range must be set. However, for rotational measurements this must be done for several different angles of the specimen. This creates two ranges for the measurement, both a range in height and a range of measuring angle. The light must be set as well; it is done the same way as described earlier. With rotation of the sample different reflections of light will occur. The light setting is as standard constant under the whole measurement. If the reflections make the light too much or too low at certain angles is there a function for it. The XSmartFlash function will perform measurements with altering light.

4.2 What measurements have been done?

During this thesis several different measurements have been done. Here will a description of each measurement be presented.

4.2.1 One sided measurements

One sided measurements is preformed to learn how to operate the microscope and to do different comparisons. Some measurements also became those that were used in FEM simulations later on. The sections below describe the different comparisons that will be done. The surfaces will be characterized by the parameters described in Section 4.5.1.

1. **Sides of the foil: Bright vs. Matt**
   Perhaps the first thing one sees when looking at a piece of aluminium foil is the appearance of the different sides. One side is bright while the other one is matt. This comparison will investigate the differences of the two sides of the foil.
2. **Different manufacturers: Manufacturer A vs. Manufacturer B**

Foils of two different manufacturers will be compared. The two manufacturers use different production technique and therefore also different alloys to produce the foil as described in Section 2.4. How does that influence the properties of the foils surfaces?

3. **Thickness of the foil: 6.30 µm vs. 9.00 µm**
   To create different thicknesses of foil the forces during production is different; to create a thinner foil more force is needed. In this comparison is it investigated if that affect the surfaces of the foil, if the different thicknesses have differences in their surface topographies.
4. **Time of production: Old work rollers vs. new work rollers**
   During production the rollers that are in direct contact with the foil, the work rollers, become worn and are replaced according to a fixed schedule. These measurements investigate if the wear of the work roller affects the surfaces of the Al-foil.

4.2.2 Rotational measurement

With the rotational measurements both sides of the foil will be measured in one measurement. This will reveal the true thickness variation of the foil. This type of measurement has not been tested before on Al-foil of the thicknesses used in this evaluation. Therefore is the primary objective with these measurements to establish a procedure for the measurement.

4.3 Filtering options

There are several filtering options available for measurements. This section will describe the different filtration possibilities.

4.3.1 F-operator

The F-operator can be applied to both line and surface measurements to remove the form. As shown in Figure 13 a measurement have been made on a spherical surface and by removing the spherical form the primary surface is revealed. The F-operator can be applied to many different forms: spherical, cylindrical, tilted plane or some curvature defined by an equation. (Michigan Metrology, 2016)

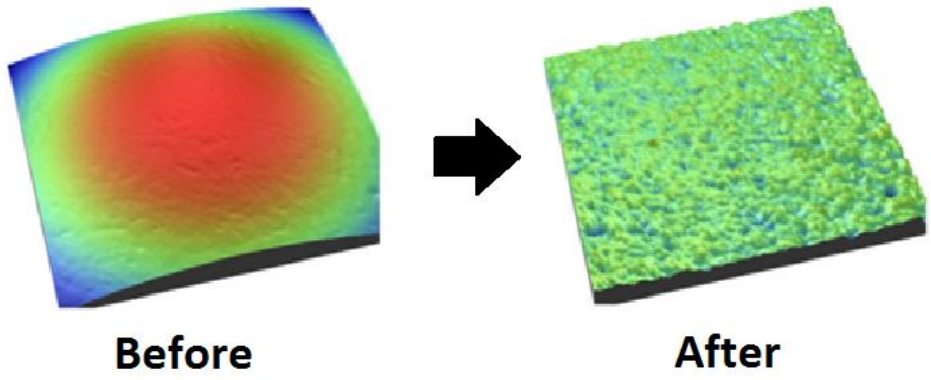

Figure 13. A F-operator applied to a surface measurement.

4.3.2 Primary, roughness and waviness profiles

The primary profile represents the true topography along the measured line, i.e. the results after the F-operator. The waviness profile represents the coarse form of the primary profile, i.e. the wavelengths longer than the cut-off wavelength, λ_c. The opposite is found in the roughness profile,

where the fine changes of the primary profile are displayed and used for calculations of parameters.

An analogy is a chart over how the temperature varies through the day and over the seasons. The daily variation can be seen as the roughness while the season variation can be seen as the waviness and the combined variation is the primary.

The settings applied to filter the primary profile are defined in the standard ISO 4288 The standard defines the cut-off wavelength. The cut-off wavelength is used both to filter the measuring result and to define the length of each section, which is described in the next section.

4.4 Line profiles

The same standard, ISO 4288, that defines how to filter the measured profile also describes how to perform the measurements. There is a defined measuring distance and it is divided into different sections. The first section is the start section (called pre-travel), then there are multiple measuring sections and it is finished with the stopping section (called post-travel). The measurements taken during the pre- and post-travel is not necessarily very reliable so they are not used to calculate the final results. The standard defines that there should be five measuring sections. For a given Ra (a roughness parameter) value of the measured line the standard specifies the single measuring length (one measuring section), the total measuring length (all five measuring sections) and the traversed length (the total measuring length plus the pre- and post-travel lengths). If the space does not allow to measure the full length of the profile the number of sections should be reduced, not the length of each section.

4.4.1 Measured parameters

Each profile has its own measurable parameters. The parameters for the primary profile will be described below. Parameters for the waviness and the roughness profile are calculated by the same formulas, the only difference is that the input has different grades of filtration. Like primary profile parameters have the prefix P, parameters for waviness will have the prefix W and roughness prefix R, e.g. Pa, Wa and Ra are similar parameters but are based on different grades of filtration of the measurement.

4.4.1.1 Pa

The Pa parameter is the arithmetical mean height of the line profile. As shown in Equation (1) the value is calculated as the mean of the absolute value of the line height over a set reference level

$$Pa = \frac{1}{l}\int_{l} |z(x)|dx \qquad (1)$$

where l is the length of one measured section. The parameter is calculated in all sections and a value for the whole measured profile is the mean of the values in all measured sections.

4.4.1.2 Pt & Pz

These parameters are associated with the maximum height of the line profile. Pz is the mean value of the heights in each section, i.e. the height from the highest peak to the lowest valley is calculated in each measured section and then Pz represents the mean. Pt is the height form the highest peak to the lowest valley of the whole measured length.

4.5 Surface measurements

A standard that specifies how to do measurements over a surface is not available like there is for line measurements. This implies that the measurements can be done with no restrictions. It is therefore important to be specific how the measurements were made. Another difference between the line and surface measurements is the filtering options. For surfaces is there only the F-operator as filtering option.

4.5.1 Measured parameters

The parameters that characterize the surface properties are very similar to those for line profiles, both by name and how they are calculated. However, for surfaces double integrals are needed.

4.5.1.1 Sa

The Sa parameter is the arithmetical mean height of the surface, see Equation (2). This is similar to the line parameters Pa, Wa and Ra. With no standard for dividing the surface into sections as there are for lines, this calculation is performed on the virgin surface directly (with area A).

$$Sa = \frac{1}{A}\iint_A |z(x,y)|dxdy \tag{2}$$

4.5.1.2 Sz & S10z

Sz represents the total height of the surface in the defined area. It is calculated as the vertical distance from the lowest valley to the highest peak. S10z is almost identical to Sz, but instead based on the mean of the ten largest peak to valley distances.

4.5.1.3 Sdr

Sdr stands for developed interfacial area ratio. It compares the physical area of the surface with the area of the reference plane, explained by equation (3).

$$Sdr = \frac{(Surface\ area) - (Cross\ sectional\ area)}{(Cross\ sectional\ area)} \cdot 100 = \frac{A - A_{ref}}{A_{ref}} \cdot 100 \tag{3}$$

For a continuous area it is calculated with equation (4)

$$Sdr = \frac{1}{A}\iint \left(\sqrt{1 + \left(\frac{\partial z(x,y)}{\partial x}\right)^2 + \left(\frac{\partial z(x,y)}{\partial y}\right)^2} - 1 \right) dxdy \tag{4}$$

For practical implementation, numerical solution methods are employed. The area is then built up by quadrilaterals ABCD at position (x_i, y_j) where $[1<i<M-1,\ 1<j<N-1]$ (where N and M is the number of measure points in each direction). Since the four corners may not be in the same plane, it is divided in to two triangles. This can be done in two ways: triangles ABC & ACD or ABD & BCD. The quadrilaterals area is calculated both ways and the average is used to represent the area. Figure 14 shows the procedure graphically.

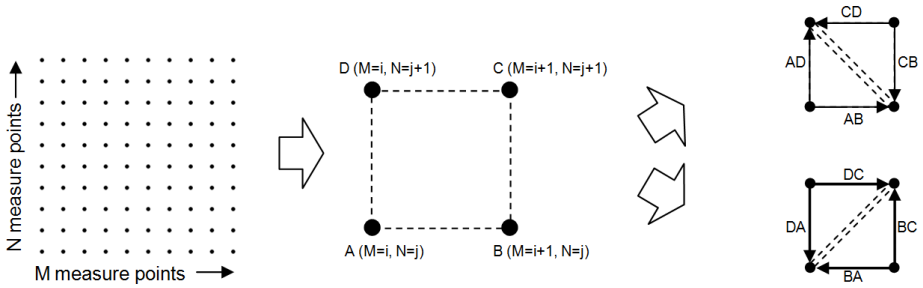

Figure 14. Procedure for calculating Sdr

Equation (5) calculates the area for each quadrilateral as the average of the two combinations of double triangle areas.

$$A_{ij} = \frac{1}{2}\left[\left(\frac{1}{2}\left|\overrightarrow{AB} \times \overrightarrow{AD}\right| + \frac{1}{2}\left|\overrightarrow{CB} \times \overrightarrow{CD}\right|\right) + \left(\frac{1}{2}\left|\overrightarrow{BA} \times \overrightarrow{BC}\right| + \frac{1}{2}\left|\overrightarrow{DA} \times \overrightarrow{DC}\right|\right)\right] \quad (5)$$

All quadrilateral areas are then summed up to give the area of the whole surface in Equation (6).

$$A = \sum_{i=1}^{M-1}\sum_{j=1}^{N-1} A_{ij} \quad (6)$$

The cross sectional area is calculated in Equation (7).

$$A_{ref} = (M-1)(N-1)\Delta x \Delta y \quad (7)$$

The surface area is the compared to the cross sectional area to give the Sdr value as described in Equation (3).

4.5.1.4 Gradient parameters

The parameters related to the gradient are the direction and slope of the gradient. The direction is calculated in the reference plane and the slope is the angle between the gradient and the reference plane. When calculated the results can be plotted against each other in a diagram. From the diagram is it possible to see if there are any clear characteristics of the measured surface. For example will the rolling lines on the bright side give the gradient concentrate in clear directions.

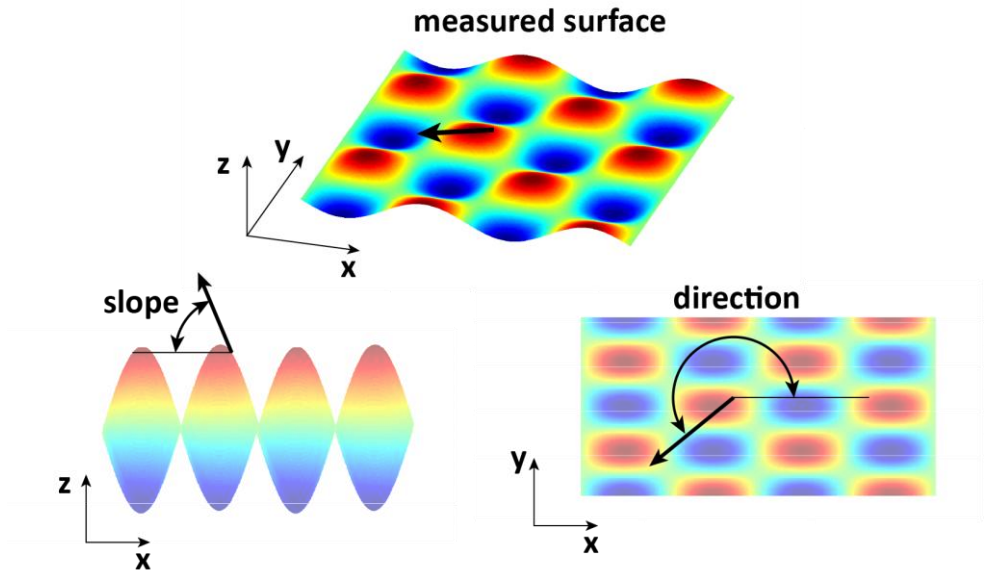

Figure 15. Example of the two gradient angles.

5 Results and conclusions of surface measurements

The results of the different measurements are presented in this chapter where. It starts off with the one sided measurements and the four different comparisons performed. Finally there is a presentation of the results of the rotational measurements.

5.1 One side measurement results

All measurements were performed with the objective lens with 50x magnification and polarized light. The resolution in all measurements is 1 µm in lateral direction and 20 nm in vertical direction. As before mentioned all measurements are done with the Alicona infiniteFocus microscope at LTH.

5.1.1 Different sides of the foil

The foil used while investigating the different sides of the foil is #1 in Table 2.

There were in total ten measurements performed, five on each side of the foil. Two representative measurements, one for each side, are presented in Figure 16 and Figure 17.

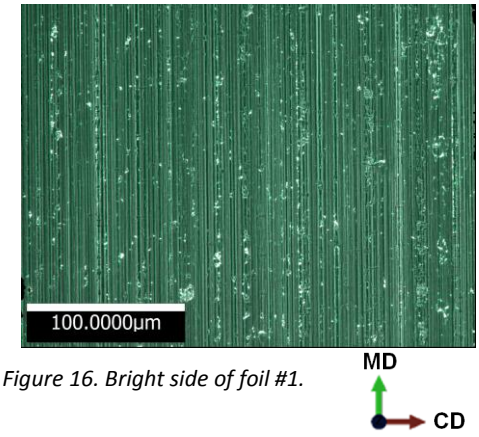

Figure 16. Bright side of foil #1.

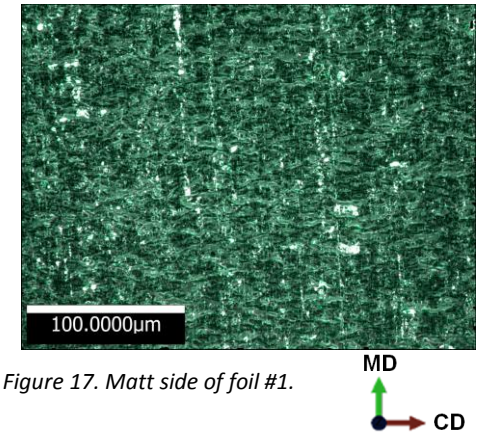

Figure 17. Matt side of foil #1.

As visible in both Figure 16 and Figure 17, rolling lines from the production are visible in MD direction. The rolling lines are very clear and the most prominent feature on the bright side. While the matt side has traces of some rolling lines visible, the most of them have vanished in the doubling process.

Applying a color range corresponding to the height of the different surfaces creates topography figures. Figure 18 and Figure 19 are the topography images of the surfaces in Figure 16 and Figure 17. The highest peaks and lowest valleys have been removed to give a clearer look of how the surface changes in height. The range represents a 95 % confidence interval (2.5-97.5%) of the height from the measuring points.

The rolling lines on the bright side are visible in the topography images as well but they are not on the matt side. The matt side shows a more arbitrary pattern that originates from the doubling process. However, some higher and lower areas can be seen along with small peaks and valleys.

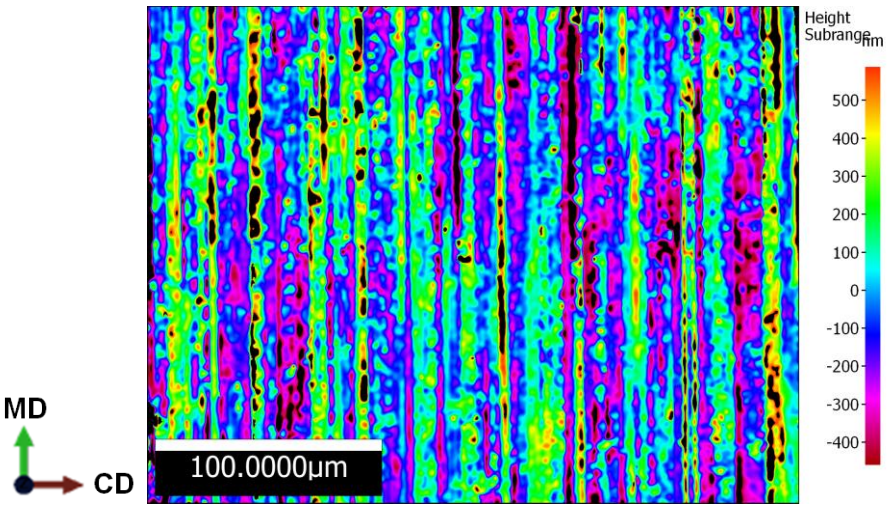

Figure 18. Topography image of the bright side of foil #1.

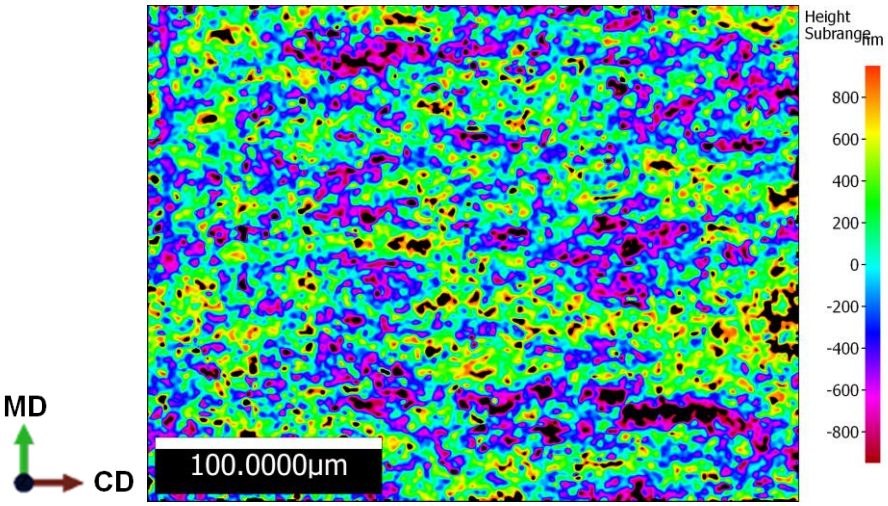

Figure 19. Topography image of the matt side of foil #1.

The gradient images presented in Figure 20 show that the bright side have a very clear directional features, i.e. the rolling lines. On the matt sides gradients have a more evenly distributed direction but with some concentrations at 90 and 270 degrees. Comparing the slopes of the gradient between the two sides shows that the matt side has steeper slopes.

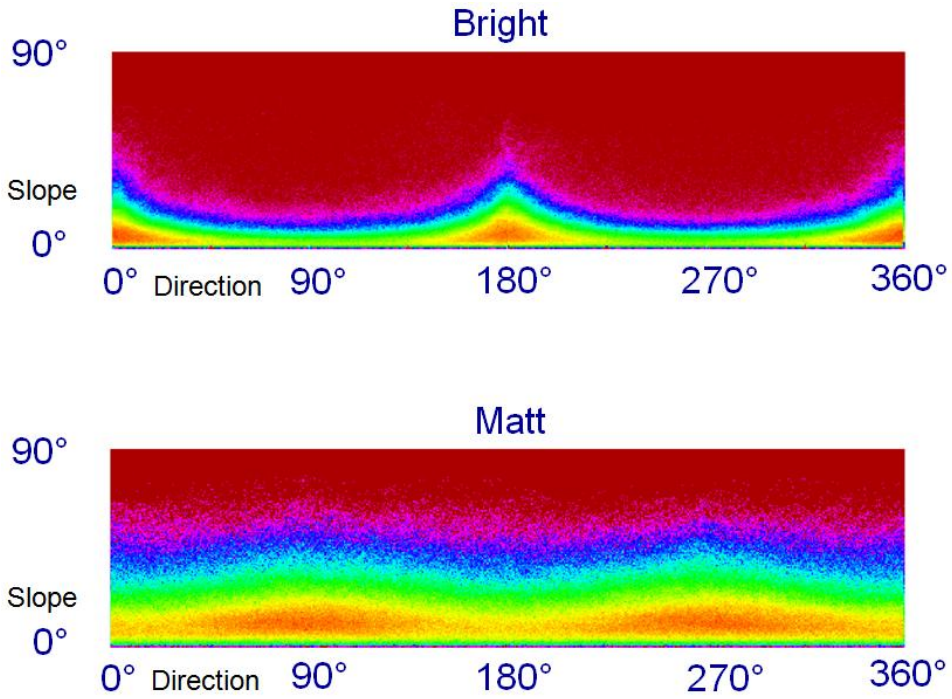

Figure 20. Gradient images of the two different sides of foil #1.

The topography image of the matt side has a larger range than the bright side. This also reflects the values of the parameters presented below. The matt side has a higher average height of its surface, as seen in Figure 21, and a higher surface offset as seen in Figure 22. The maximum height values in Figure 23 show also that the matt surface is coarser. However, for a foil of 9 µm thickness to have a surface height variation that high as presented in Figure 23 seems improbable.

The values of the parameters presented in this comparison are the average of the five measurements done on each surface. All values from the ten measurements can be found in Appendix B.

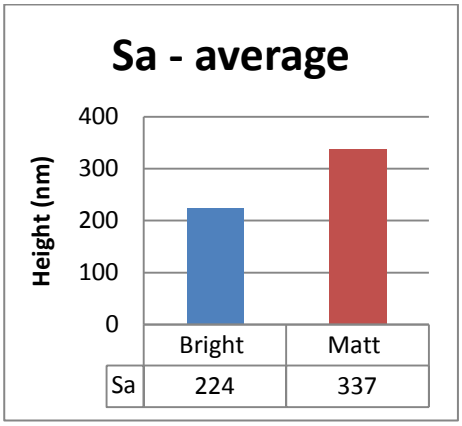

Figure 21. Sa values for foil #1.

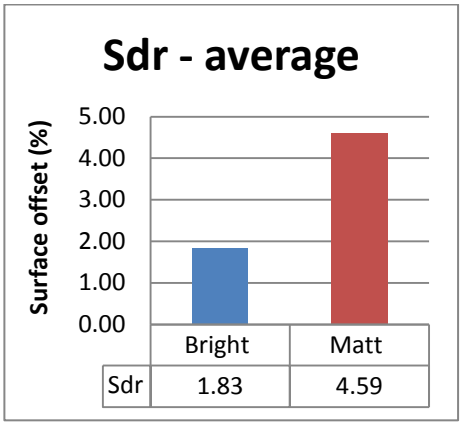

Figure 22. Sdr values for foil #1.

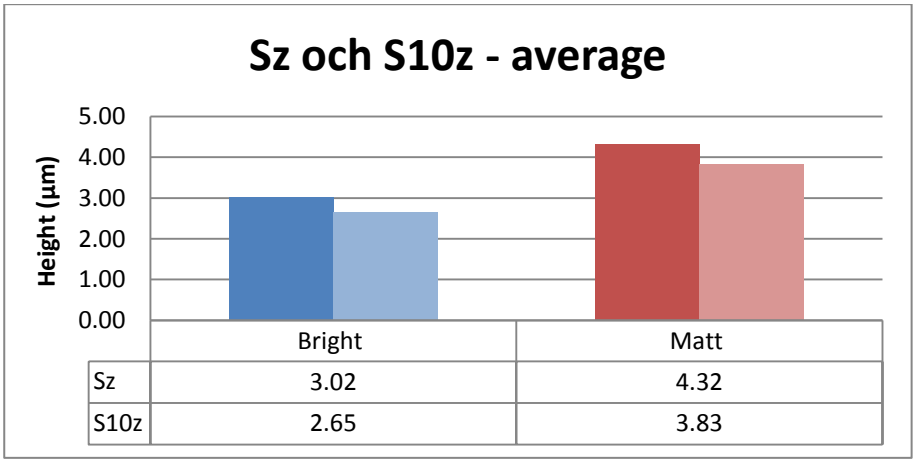

Figure 23. Sz and S10z values for foil #1.

The bright side shows very clearly roll marks from the production process and they characterize the surface topography. The matt side does not have any characterizing pattern but there seems to be some directional concentration perpendicular to the direction of the rolling lines on the bright side. The steeper slopes on the matt side tends to be related to the larger height of the surface. The improbable results of the Sz and S10z parameters do that they will not be used any further.

5.1.2 Foil from different manufacturers

This section compares the foils #1, #2, #3 and #4, see Table 2. Those are foils of two thicknesses from two different manufacturers. In this section, only the manufacturers will be compared, the foils have the same thickness. This comparison is only based on one measurement on each side.

All bright surfaces in these measurements look alike, so do the matt surfaces. Therefore will no images of the different surfaces be presented.

Figure 24 and Figure 25 compares the 9 µm foils manufactured by manufacturer A and B. Consistent with the previous comparison, the matt surfaces are coarser than the bright surfaces. The foil produced by manufacturer B has finer surfaces than the foil produced by manufacturer A.

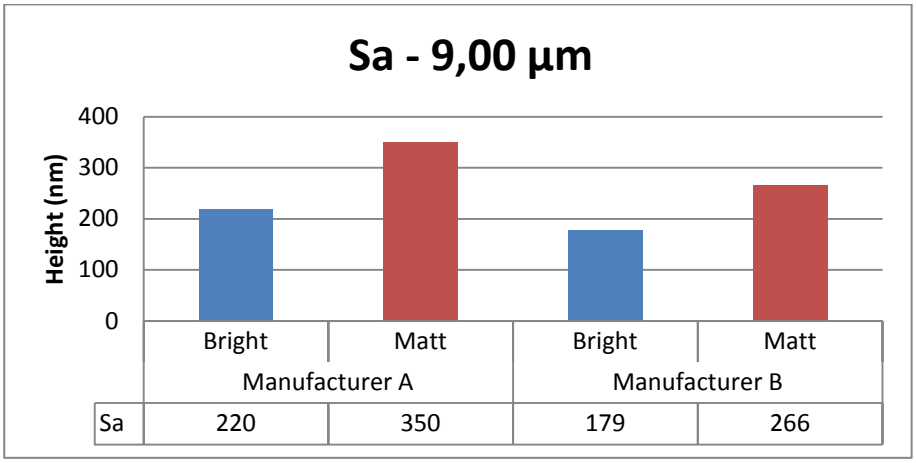

Figure 24. Comparison of Sa values between 9µm foil of different manufacturers (#1 and #3).

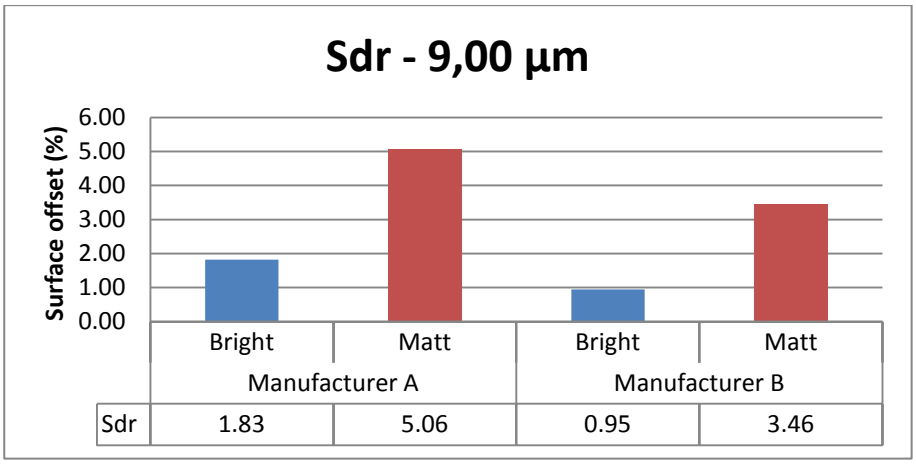

Figure 25. Comparison of Sdr values between 9µm foil of different manufacturers (#1 and #3).

The same comparison has been done for both manufacturers 6.3 µm foil (Figure 26 and Figure 27). The same results can be found in this comparison. The surfaces of manufacturer B's foil are finer than those of the foil of manufacturer A. However, the parameter values are based on only one measurement on each side. These differences can be within the standard deviation of the surface variation.

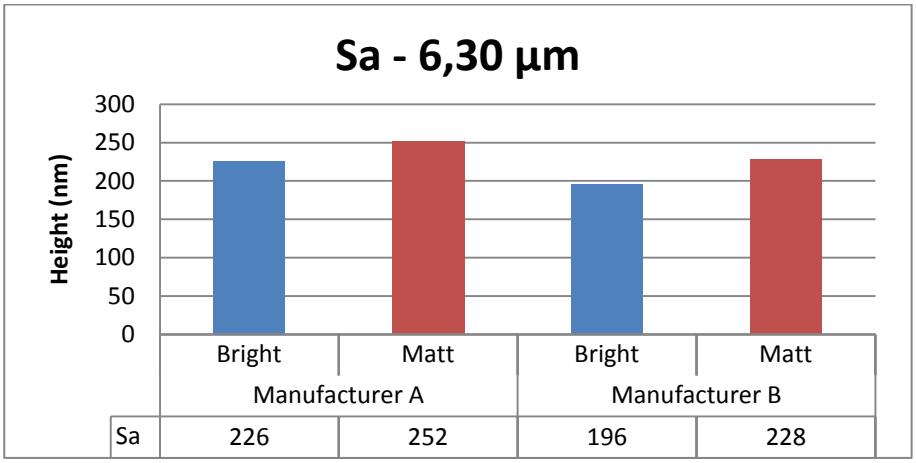

Figure 26. Comparison of Sa values between 6,3µm foil of different manufacturers (#2 and #4).

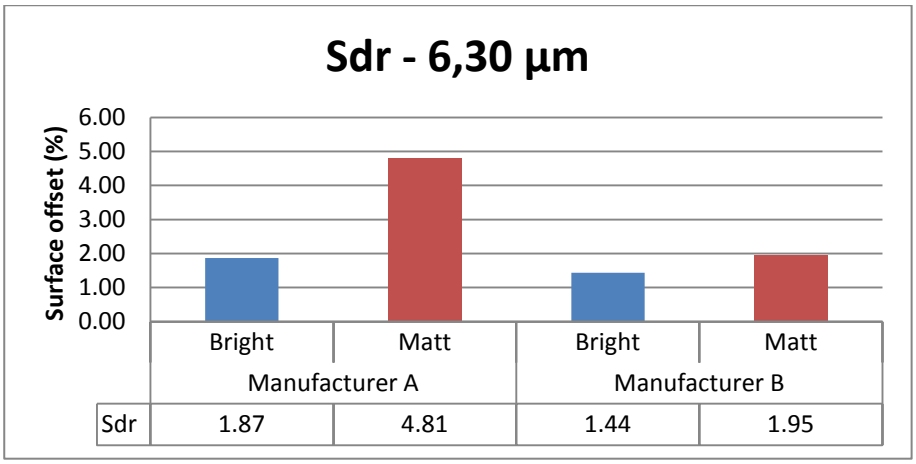

Figure 27. Comparison of Sdr values between 6,3µm foil of different manufacturers (#2 and #4).

5.1.3 Foil with different thicknesses

The comparison between the different foil thicknesses have been done with the same measurements as in the comparison between different manufacturers.

Parameter values of the two foils of different thickness from manufacturer A is presented in Figure 28 and Figure 29. Both parameters show fairly consistent values comparing the bright side of both foils. On the matt side the thicker foil have an increase on both parameters compared to the thinner foil.

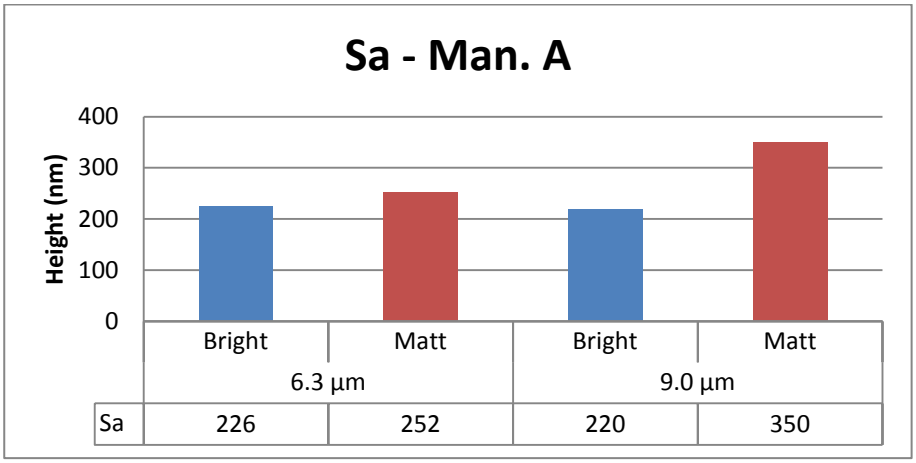

Figure 28. Comparison of Sa values between foils from manufacturer A of different thickness (#1 and #2).

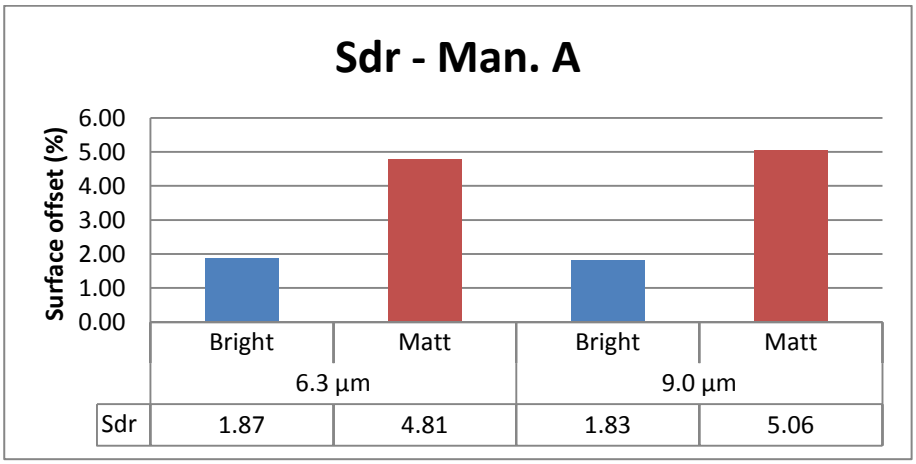

Figure 29. Comparison of Sdr values between foils from manufacturer A of different thickness (#1 and #2).

There are similar trends for the different foils of manufacturer B as for manufacturer A, as shown in Figure 30 and Figure 31. The matt surface is coarser for the thicker foil. The bright side tends to be finer on the thicker foil for manufacturer B.

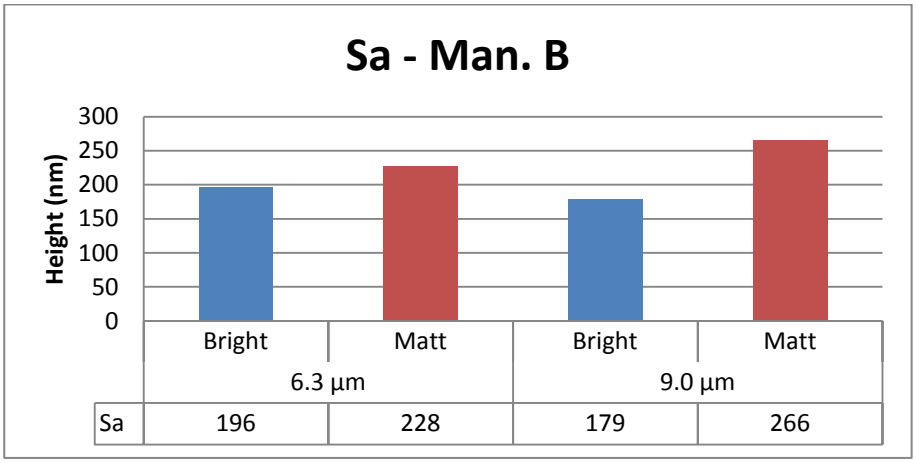

Figure 30. Comparison of Sa values between foils from manufacturer B of different thickness (#3 and #4).

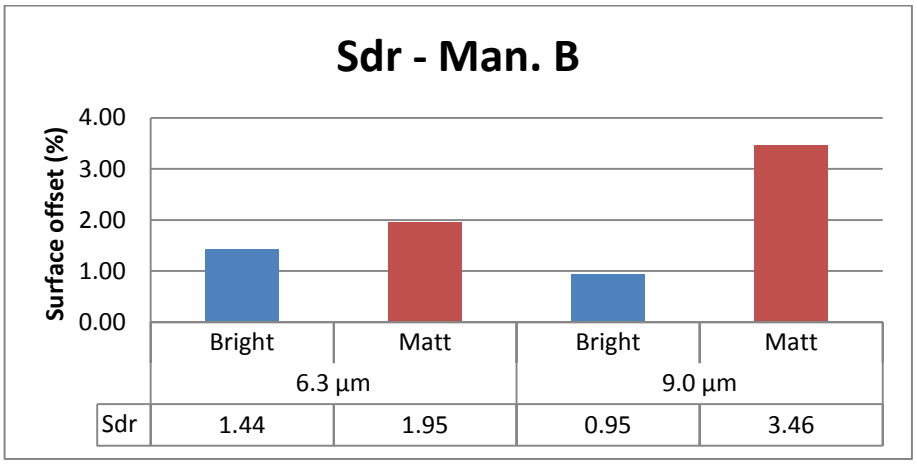

Figure 31. Comparison of Sdr values between foils from manufacturer B of different thickness (#3 and #4).

Over all in this comparison the bright side's parameter values stays consistent or become slightly finer on the thicker foil, while the matt side has a trend to get coarser on thicker foils. However, the parameter values are based on only one measurement on each side. These differences can be within the standard deviation of the surface variation.

5.1.4 Different wear on work rollers

The foil used in this comparison is foil #5 in Table 2. Measurements of a piece of foil from the production with a newly grind work roller will be referred to as new. Measurements on a piece of foil made by a worn work roller will be referred to as old.

Five measurements where preformed on each side. In the report, only the average of each parameter will be presented, all individual measurements are available in Appendix C. The bright side of a foil produced by a new work roller is visualized in Figure 32. Figure 33 is the corresponding image for a foil produced by a worn work roller. The foil produced with new work rollers has clearer

rolling lines on its surface while on the surface produced with old work rollers they are more diluted. On the matt surfaces are there no visible differences.

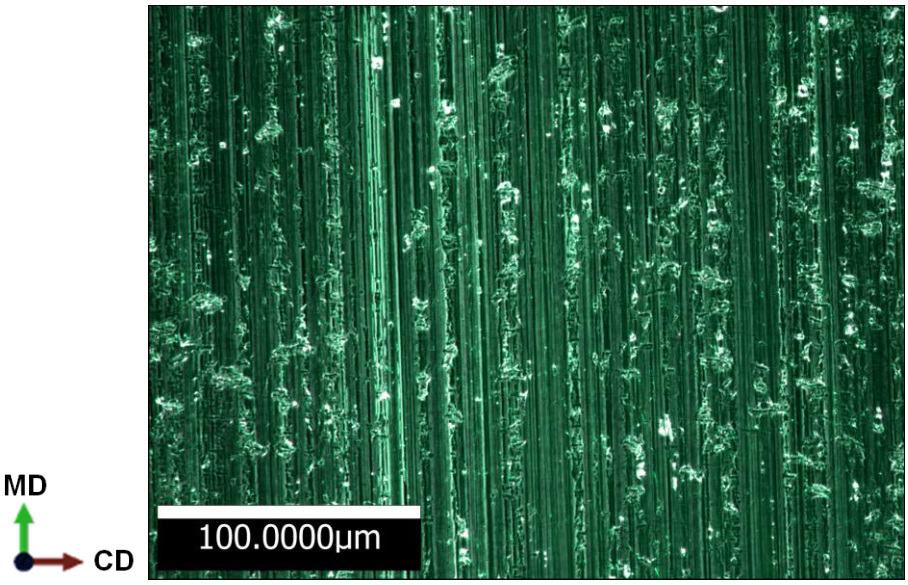

Figure 32. Bright side produced with a new work roller.

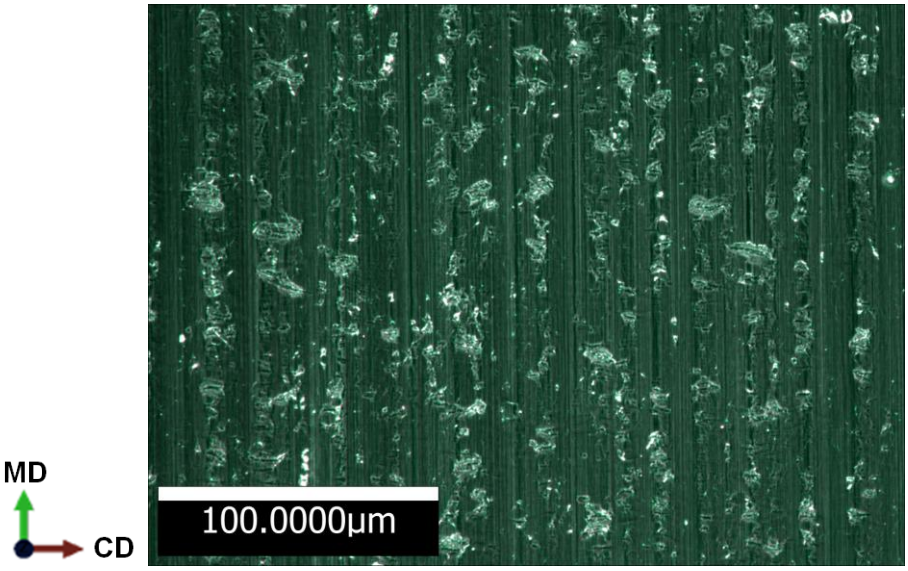

Figure 33. Bright side produced with an old work roller.

Figure 34 and Figure 35 present line profiles extracted from the two images above. They show the height profile of the surface from left to right in the middle of Figure 32 and Figure 33. Note the difference in scale of the two axes in each figure. They are fairly similar in height with the addition of spikes on the line representing the foil produced with new work rollers. The spikes in negative

direction are logical and are a trace from the production. The newly grind work rollers have ridges that makes a mark on the foil surface. When the ridges get worn the deep marks on the foil disappears.

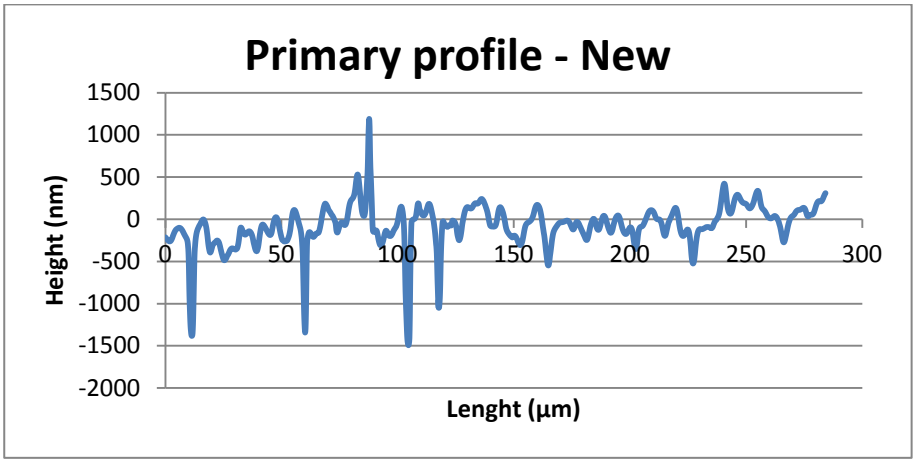

Figure 34. Line profile from foil produced with new work rollers.

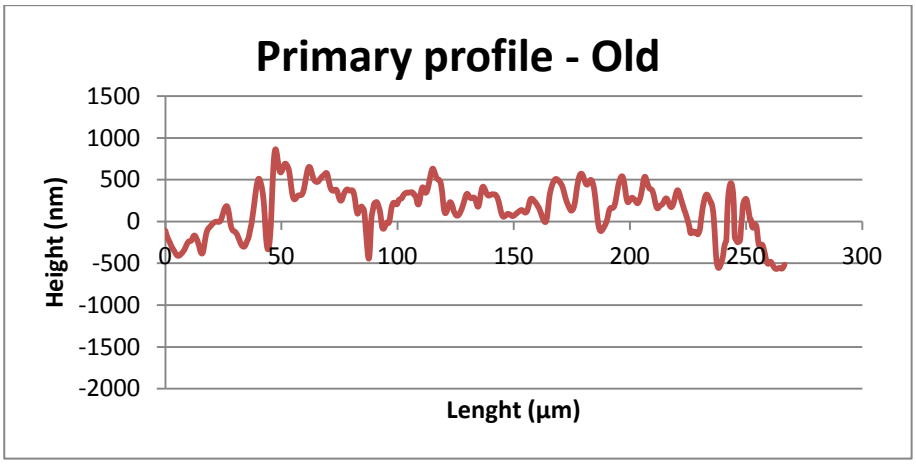

Figure 35. Line profile form foil produced with old work rollers.

After establishing that there are different looks on the bright surfaces, it comes as a bit of a surprise when comparing the surface parameters. As shown in Figure 36 and Figure 37 there are not much difference between the surfaces of the foils produced with differently worn work rollers.

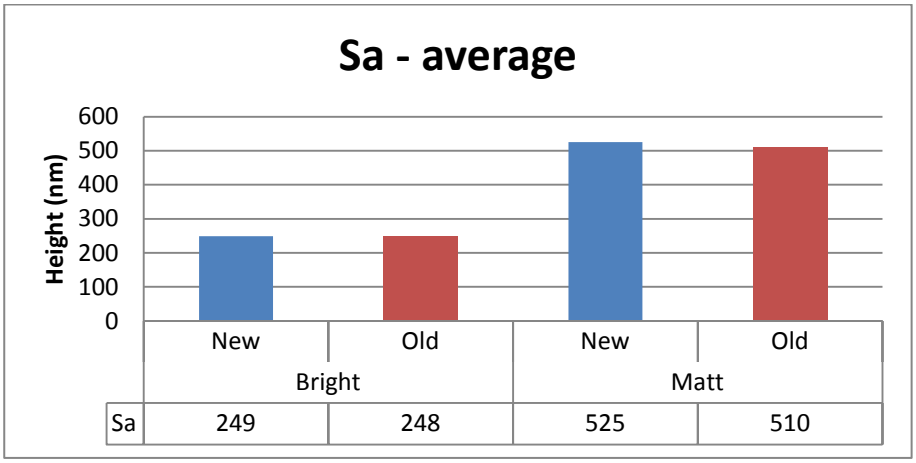

Figure 36. Comparison of Sa values on different sides between foils from different time of production.

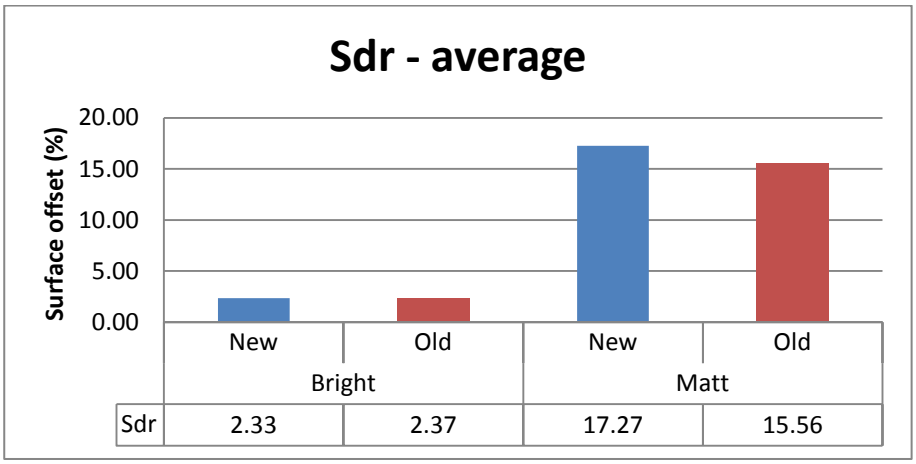

Figure 37. Comparison of Sdr values on different sides between foils from different time of production.

It seems like the wear of work rollers have no influence on the surface parameters. However, the surface topography changes with the wear of the work rollers. A more worn work roller creates less clear rolling lines on the surface.

5.2 Rotational measurement results

Unfortunately, none of the attempts to perform rotational measurement gave any results. Many attempts with many different setting were tried. Different angles of the specimen, different light settings, both with and without the XSmartFlash setting and polarized light. The different foil holders were tried multiple times. Due to the long acquisition time for a rotational measurement, typically several hours, not that many attempts could be performed. In Section 8.2.3 the failed attempts and further possibilities will be discussed.

6 Virtual testing of surface measurements

The surface measurements will now be used in FEM simulations. This is to investigate if there is a correlation between the surface topographies and the mechanical strength of the foil. Therefore will a simulated tensile test be performed on pieces with surfaces measurements. The discovery that the direction of the surface features is perpendicular to each other on the two sides raised bi-investigation for the simulations. How does the perpendicularity affect the models?

This chapter will describe the models simulated. Starting off with the mesh creation, followed up with the material model and ending with a description of the different boundary conditions implemented.

6.1 Simulated meshes

Measurements previously done on foil #1 in Table 2 were transformed to meshes as shown in Appendix A. The element size was chosen to be approximately 1.5 µm. The simulations would be done in three different directions (MD, 45° and CD) to correlate to earlier work at Tetra Pak (Käck & Malmberg, 2015). Therefore were two different meshes created initially, see Figure 38, both in the size of 100 by 100 µm and with a thickness of 9 µm. Because the mesh was created in a quadratic shape the same mesh could be used for two models, with tension in MD or CD.

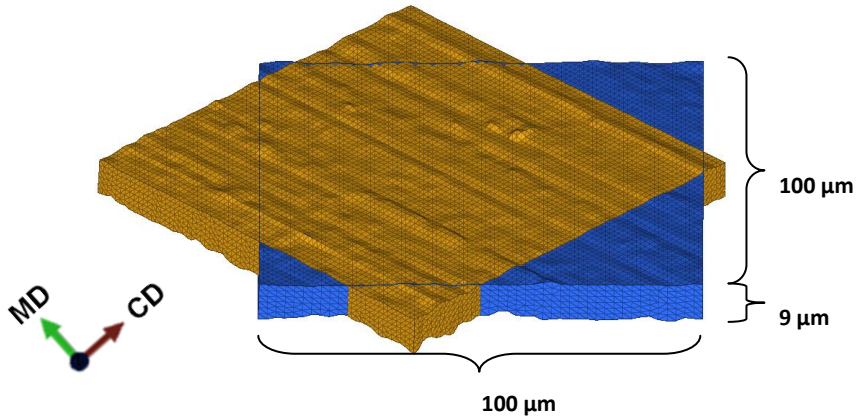

Figure 38. Meshes for tension in MD or CD (brown) and 45 degrees (blue).

After the first simulations, it was considered that some extra material was needed to get rid of some side or edge effects that occurred in the simulations. The extra material was added to the top and bottom sides of each models mesh, see Figure 39. This material made the ends of the meshes into rectangles with straight edges instead of edges with the shape of the surface topographies as there were before.

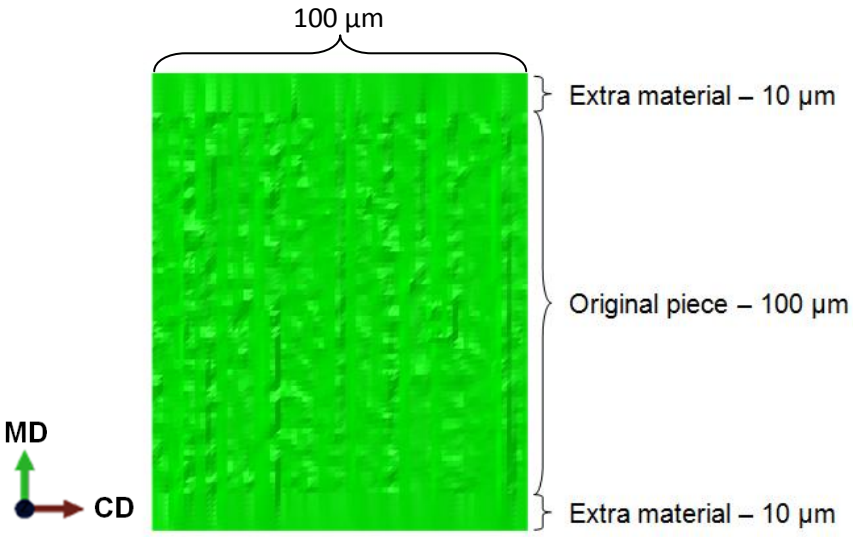

Figure 39. The second mesh, with extra material, for simulations in MD-direction (rolling lines visible from top to bottom).

The choice of elements was primary first-order tetrahedral elements (Element name: C3D4). The file format used to export the surfaces from the microscope, STL, uses triangles to represent the measured surfaces. Therefore was brick shaped elements ruled out. After realizing first-order tetrahedral elements does not work well in structural analysis as the element is regarded too stiff (Dhondt, 2014) the elements were changed. The new elements were second-order tetrahedral elements (C3D10M). Figure 40 visualizes the difference between the different types of elements.

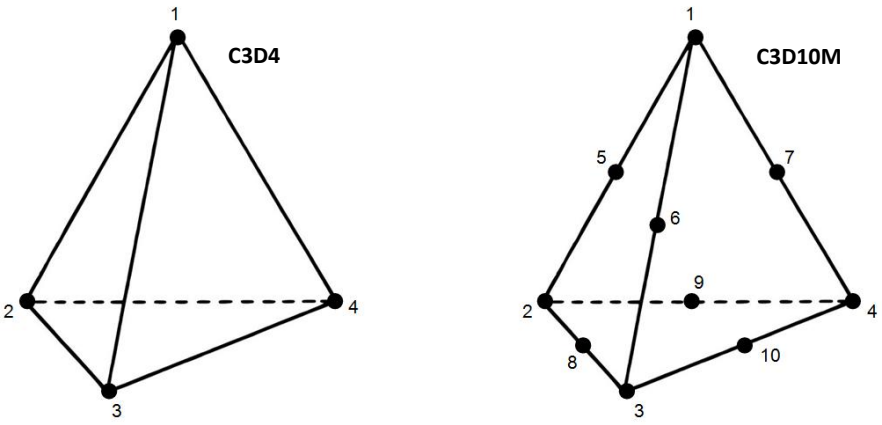

Figure 40. Tetrahedral elements with four and ten nodes.

6.2 Material model

The material model that is utilized originates from physical tensile tests performed at Tetra Pak . The experimental procedure is described in (Käck & Malmberg, 2015). From macroscopic tensile test results it is possible to fit the analytical expression proposed by Ramberg-Osgood's material model, equation (8)

$$\epsilon = \frac{\sigma}{E} + \left(\frac{\sigma}{E_0}\right)^N \tag{8}$$

where E_0 is the strain-hardening modulus and N is the strain-hardening exponent (Mäkelä, 2012). The material parameters are possible to identify directly from the experimental curve. The model is extrapolated to account for the local effects, see Figure 41. Experiments at Tetra Pak in micro scale have shown tension locally can reach over 200 %. If this is not done and the strain surpasses the material model ABAQUS will assume ideal plasticity, i.e. a horizontal line in the stress-strain diagram.

The elastic modulus is set to 36 GPa which is roughly half of the normal value of aluminium that is normally around 70 GPa. The reason for the low value is at Tetra Pak assumed to be due to the thin foil. 9 µm foils have only a few or sometimes only one grain across the thickness which leads to other material parameters than in thicker goods.

The material model is also set to be an isotropic model to start with. This assumption is made to get a simplified model. If there is time an anisotropic model will be implemented.

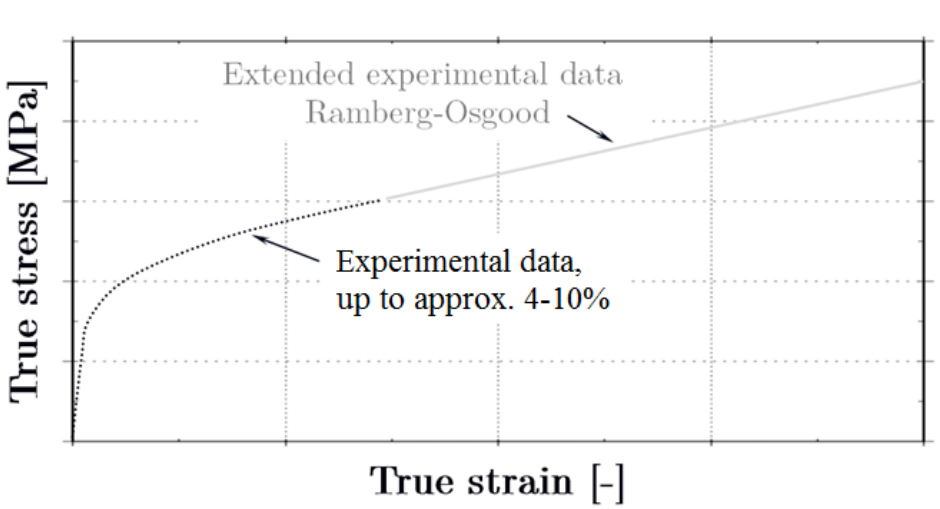

Figure 41. Visualization of the material model extrapolation.

6.3 Boundary conditions

The small piece of foil that is modeled in this thesis is thought to be part of a strip of Al-foil being put through a tensile test, see Figure 42. Some different set ups of boundary conditions were tested, but in the report only a couple of them will be presented.

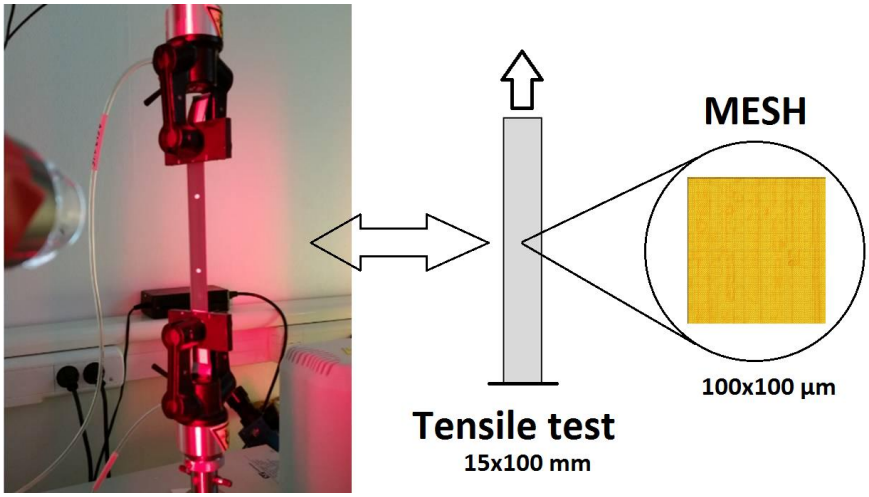

Figure 42. Origin of the boundary conditions.

The first set of boundary conditions is represented to the left in Figure 43. The bottom surface is fixed in Y-direction and the left surface is fixed in X-direction. In the bottom left corner where the two earlier conditions meet one node is fixed in Z-direction (depth). That only one node is fixed in Z-directions is considered sufficiently though there is nothing making the model move in Z-direction. This condition is only to prevent rigid body motion of the mesh. The movement in the model derives from the displacement in positive Y-direction of a reference point, i.e. the models are displacement controlled. The reference point is connected to the nodes on the top surface with a coupling. The coupling is fixed in Y-direction, i.e. the top surface moves uniformly in Y-direction. To prevent rigid body motion of the reference point are all other degrees of freedom related to it fixed.

The second set of boundary conditions is represented to the right in Figure 43. It uses the same conditions as in the first set plus one extra. The added boundary condition is the one on the right side. It prevents movement of the nodes on the right side in X-direction relative to each other. The right side nodes can move in X-direction but they all move the same distance in X-direction.

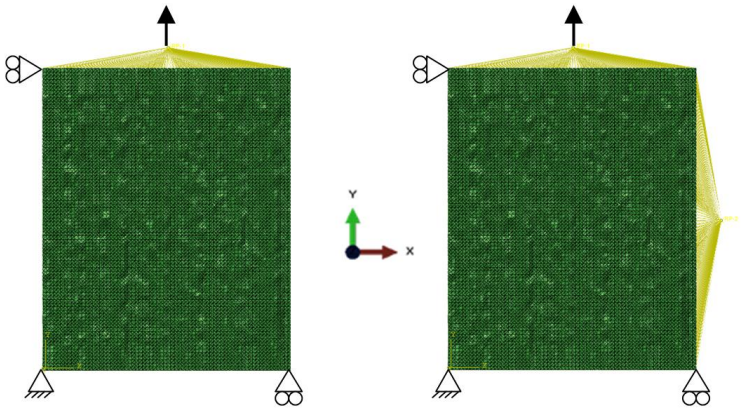

Figure 43. Two different sets of boundary conditions used in the simulations.

7 Results and conclusions of virtual testing

In this chapter will the results and conclusions of the simulations be presented. The iterative process is reflected by the results. It starts out with the less successive simulations to then end up with the most trustworthy simulations.

7.1 Early simulation results

The first simulations were done with the first set of boundary conditions and with first order tetrahedral elements (C3D4). No extra material was added to the mesh. A result of a simulation of tension in MD is seen in Figure 44. There are two prominent features of the result. First have the piece necked in width and not in thickness. Second, the stress distribution does not represent the distribution that should take place in tensile tests, with high stresses in the lower left corner and low stresses in the top left corner. Simulation of the models with tension in 45° and CD direction gave similar results.

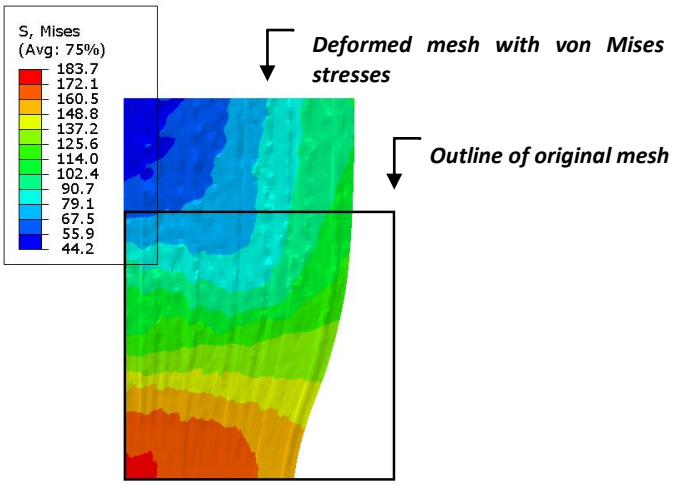

Figure 44. One of the first simulation results.

These features lead to some changes in the models. The boundary conditions were complemented by one additional on the right side. This change created the second set described in previous section. The odd distribution of stressed might be due to edge effects in the model. Therefore was extra material added to the models meshes.

Wanting to resemble a small piece of a big tensile test these results seems much more correct, uniformly deformed from a top view with local thickness deformation. In the MD model (left in Figure 45) a band of high strain has started to form across the lower part of the sample. A similar effect is visible in the 45 degree sample (middle in Figure 45). There is however the band at an

angle almost perpendicular to the rolling lines. In the CD model (right in Figure 45) no clear strain band has formed and the local strains are lower compared to the other models.

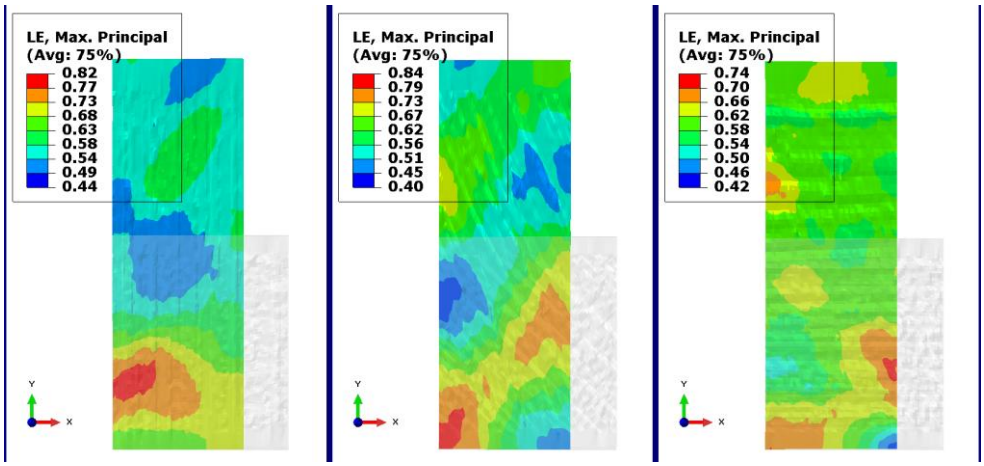

Figure 45. Strains at 100 µm displacement in MD, 45° and CD direction, respectively. The original meshes are shaded.

One conclusion was made from these simulations. The matt side's bigger topography difference affects the strength more than the bright side's topography.

Further simulations were made with these models. The change in the models was that the displacement was doubled. Those results are found in Figure 46.

During the next 100 µm displacement the band of high strain in the MD model spread. It spread across the whole width and necking of the thickness started to occur. However, the thickness just got a little bit thinner. Then the necking started to spread downwards, i.e. propagating necking. At 200 µm displacement the propagating necking has spread to the bottom edge. The strain band in the 45° model also spread with further displacement. However, it did not create the same propagating necking as in the MD model. Despite the lack of propagating necking the thickness did not get much thinner. For the CD model not much really happened with the extra displacement. The strains increased almost uniformly over the whole model.

The high strain concentrations in the MD and 45° models lead to other areas in the model get lower strains. The MD model has both the highest and the lowest strains.

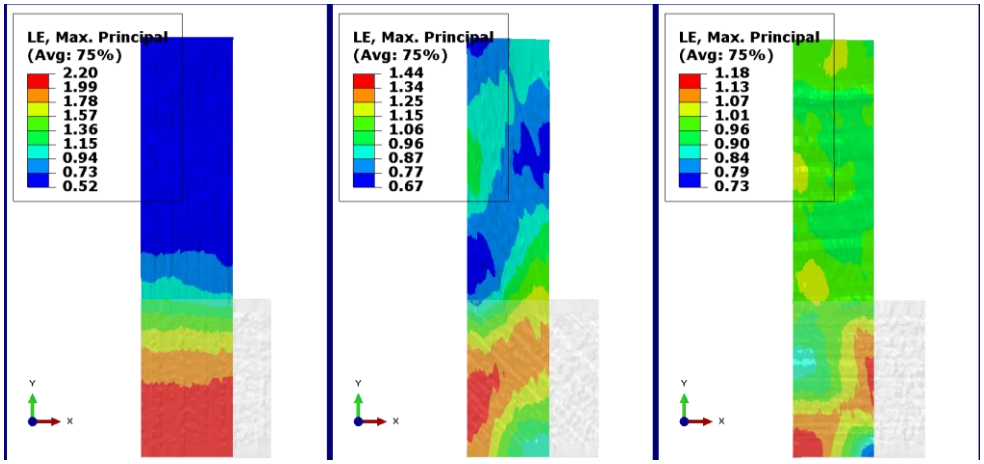

Figure 46. Strains at 200 µm displacement in MD, 45° and CD direction, respectively. The original meshes are shaded.

At this stage it was realized that the elements, C3D4, is not suitable for this application. The meshes were changed. From now on they consist out of C3D10M elements.

7.2 Final simulation results

The models became much more realistic after changing the element type to C3D10M. All models necked in clear bands across the whole width and there was no propagating necking. In Figure 47 the MD model has necked in the same place as the high strain band formed in previous models. Since these elements are less stiff they can deform more and a clear neck forms. Both in the 45° model in Figure 48 and the CD model in Figure 49 a zigzag pattern of necks have occurred. The 45° model has necked much more in one line than the others. While in the CD model necking has developed uniformly in the zigzag pattern. The displacements declared in each caption of Figure 47 to Figure 49 are the last displacement ABAQUS could calculate an equilibrium for each model.

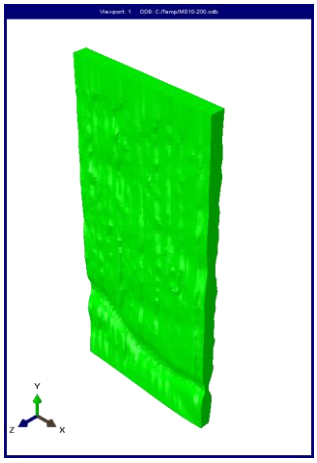

Figure 47. MD model at 58 µm displacement.

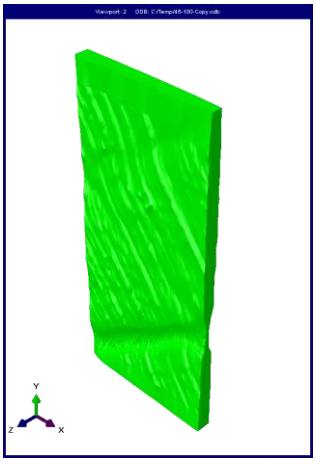

Figure 48. 45° model at 64 µm displacement.

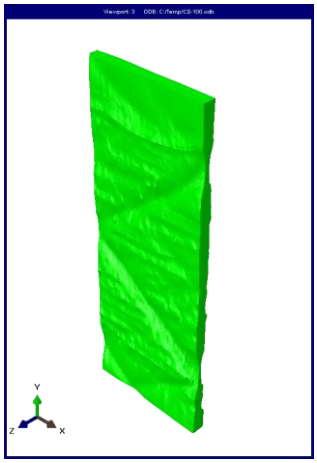

Figure 49. CD model at 91 µm displacement.

The strain of the model is visualized in Figure 50 to Figure 52. The maximum strains are located in the necking regions. All three maximum values are well above 200 % strain and all along the necking are there strains well over 100 %. The surrounding areas of the necks show moderate strain values. In the 45° model is the zigzag pattern now more obvious.

In Figure 53 a cross section of the necking in the MD model is shown. The arrows compare the thickness of the foil with the width of the necking. They form a ratio of 1:2.5. It can be compared to measurements that have been done on one edge from a failure in a tensile test. It showed a 1:2 ratio.

Figure 54 shows the force-displacement diagram produced by the three simulations done with C3D10M elements. The necking in the MD and 45° models show up as dips in the force needed. The necking in the CD model took place gradually; additionally it did it in multiple lines. The gradually necking might be the reason that this simulation could be simulated so much longer without be aborted.

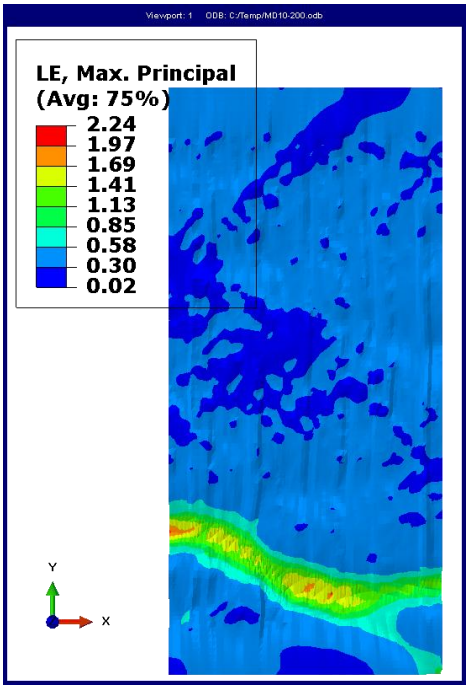

Figure 50. Logarithmic strains of the MD model at 58 µm displacement.

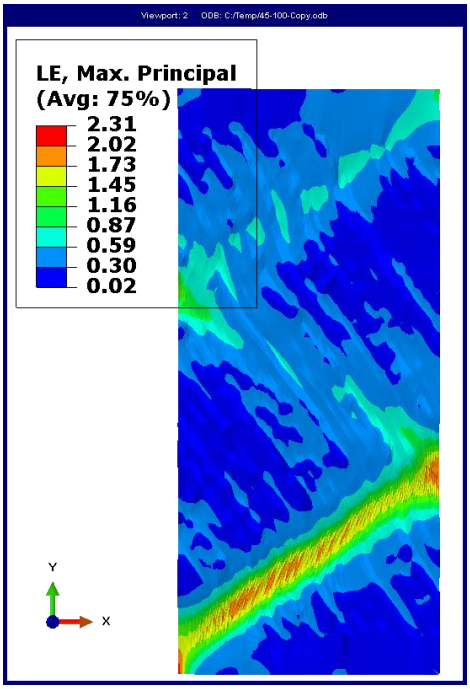

Figure 51. Logarithmic strains of the 45° model at 64 µm displacement.

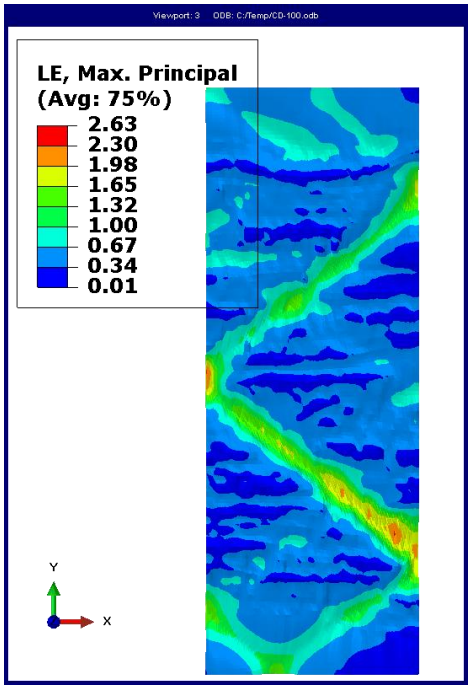

Figure 52. Logarithmic strains of the CD model at 91 µm displacement.

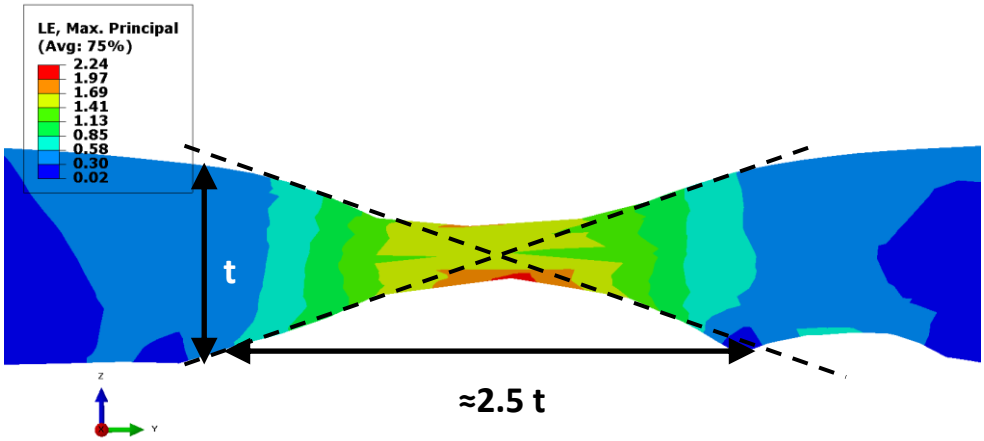

Figure 53. Cross section of the necking in the MD model at 58 µm displacement.

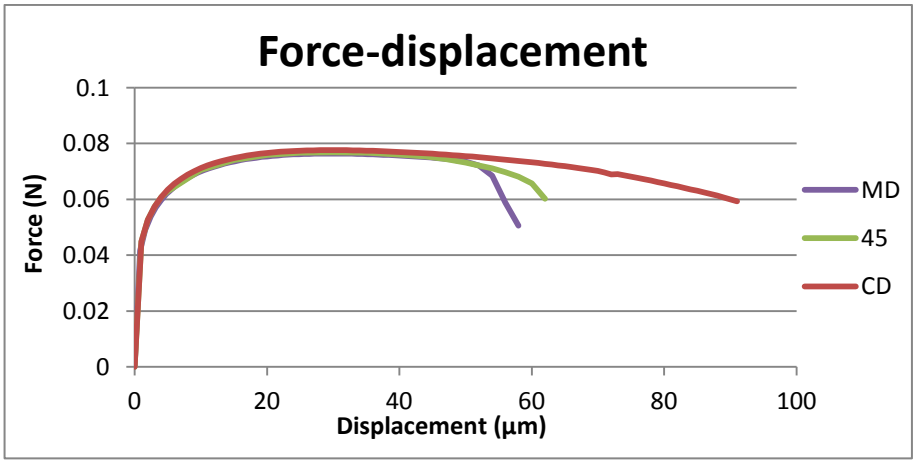

Figure 54. Force displacement diagram over the three models with C3D10M elements.

8 Discussion

This chapter will contain the discussion of this thesis. It starts with the discussion about the performance of the microscope used. Continuing with a discussion about the measurement results in different subsections and ending with a discussion about the results from the simulations.

8.1 Measurement method

The Alicona InfiniteFocus microscope is a microscope that was very easy to use. The software that controls the microscope is very intuitive. However, one big question in the beginning was which settings on the microscope should be used. The measurements were in the beginning of the project, made with both the microscopes 50x and 100x objective lenses. The measurements had some differences if the two objectives were compared. Further investigation took place to determine why these differences appeared, but no explanation was found. After it was determined that the objective lenses gave different results the settings where held constant.

8.2 Measurement results

This section has been divided into several subsections to discuss the different results from the measurements.

8.2.1 Surface images

Just by looking at the images taken of the foil some questions arise. How come that there is something that look like rolling lines visible on the matt side of the foil (see Figure 17)? What are those dots visible on both sides of the foil (e.g. Figure 16)?

The lines in MD direction visible on the matt side of the foil (Figure 17) probably originate from rolling lines. It might be that the alumina that have concentrated in lines during the early rolling of the foil. When the doubling process occurs the concentrated lines remain on the surface and look like rolling lines.

The dots both surfaces contain are a little mystery. Many different ideas have been discussed with employees at Tetra Pak. An early suggestion was that it would be particles that have not been washed away. If it would have been particles they would have made a clear mark on the topography images. On the topography images no such differences can be found. Other suggestions have been that it is concentrations of different parts of the alloy: concentrated Iron, concentrated Silicon or a concentrated combination of the two alloying metals. It might also be concentrations of alumina or pure aluminium.

A solution to these questions can be found with a SEM microscope. The interaction between the electrons and the specimen creates x-rays which can be registered. Different materials releases x-rays at different energy levels.

8.2.2 Surface parameters

The result that the bright surface is smoother than the matt side seems reasonable. I have always had the impression that the bright surface is smoother than the matt surface, just because the bright surface reflects more light than the matt surface.

The surface parameters measured in the comparison between the different sides are hard to relate to. The height differences is much smaller than what eye can see or what the skin can feel. It is only possible to relate the parameter values to the thickness of the foil. Comparing the Sa values (Figure

21) and the topography images (Figure 18 and Figure 19) with the thickness of 9 µm make the parameter values seem plausible.

However, what not seems plausible are the Sz and S10z values (Figure 23). Those feel a bit too large to represent the surfaces of a 9 µm foil. It was therefore chosen not to present any further values of Sz and S10z. Outliers in the measuring result would have a big impact on the result of these parameters.

That the Sdr value is larger for the matt surface is a little bit surprising. With this value the height differences probably have a big influence. In the topography image of the matt side (Figure 19), there are what can be referred to as waviness and roughness. The areas of higher and lower surface can be called waviness. The small height differences located over the whole surface can be seen as roughness. The combination of these features along with the larger height difference probably makes a larger Sdr value for the matt surface.

The gradient images (Figure 20) gave possibly the most interesting result. That the bright side had a clear concentration of gradients is no surprise with all those rolling lines. Unexpectedly the matt side shows concentrations of gradients as well. The matt side does not have the same concentration of gradients as the bright side. However, there are still gradients concentrated in one direction. The directions from the concentrated gradients on the two sides of the foil are perpendicular to each other. Questions arose with this result. Does this result correlate to the amount of strain possible in each direction during a tensile test? Can the matt side create bands of thinner foil across the specimen with tension in MD direction? Does the bright side behave the same with tension in CD? Do the two perpendicular directions work against each other at tests in 45 degree direction and therefore allowing more strain before fracture?

The reason for the matt side having a direction perpendicular to the bright is not known. It might be due to the lubrication in the doubling process. The theory is that the lubrication droplets get trapped between the foils, in the region between the rollers. Very high pressure will build up as liquids are incompressible. The lubrication travels in a direction of least resistance, i.e. perpendicular to the rollers. Thus, a pattern is present in this direction on the foils matt surface.

The results for the investigation of different manufacturers and different thickness are less reliable than the other results. In these two investigations only one measurement was performed on each side of the foil, i.e. there are no statistical certainty. That the foils produced by manufacturer B have smoother surfaces compared to manufacturer A might not be the case. However, by information given by Tetra Pak this result seems plausible. The alloy that manufacturer B uses for their foils is less ductile than the alloy manufacturer A uses. A ductile and softer material allows for more distortion of the surface and therefore becomes coarser.

The results for the different comparisons are often very similar; the Sa values do not change much in between some results. With only a few measurements done and a vertical resolution of 20 nm the conclusions made might not be that reliable. The differences in result are sometimes lower than the vertical resolution in which case it is within the error margin of the measurements.

In the investigation of different wear on the work rollers the Sdr values for the matt side are like no other results. The matt side resulted in values of 15.56 and 17.27 % for the foil made with old and new work rollers, respectively. Other Sdr results for the matt side have been around two to five percent. The peculiar thing is that it is not a single measurement that has produced a faulty (too high) value. Those high numbers have been calculated as an average of 5 different measurements. All measurements in this investigation were done in one day so the faulty result is probably consistent and the comparison between the two foils should be okay.

Both line and surface parameters can be used to characterize a surface, as described in Section 1. I found several reasons for using the surface parameters. First that surface measurement contains much more data points. With increasing data points the influences of an outlier diminish. Second, if

the standard for calculating line parameters would be followed the measurements done would not be sufficient. A longer line than the width of the image would be needed. Images consisting of several frames can be done but would take longer time to perform, time that not was available within this thesis.

8.2.3 Failed rotational measurements

There were no successful rotational measurements during the work of this thesis. The biggest problem was to get a correct light setting. Aluminium foil is very reflective and the surface is very smooth on a macro scale. This means that the foil behave almost as a mirror. At one measuring angle too much light gets reflected back into the microscope, while at another angle the light gets reflected away from the microscope resulting in too little light reaching the sensor. The ring light that is part of the Alicona InfiniteFocus standard equipment was used to prevent this problem. Still when light hit the sample from different angles there was a too big light differences for the microscope to complete the measurements. Another setting that is available on the microscope is the XSmartFlash function. It is a function that performs the measurement with variable light settings. This setting makes the measurement even more time consuming. This is since every image of a certain angle and height must be taken with many different light intensities. Due to the vast increase of measuring time this was only tried once.

A function that was not available could be a solution to complete a rotational measurement. This function can stitch together several measurements. If several measurements would be done in neighboring areas around an edge of the foil they could possibly be stitched together to one. However, it might be that the surface of the foil is to smooth for this function to work.

Another alternative for measure both sides of the same spot can be to use a reference that can be seen from both sides, e.g. a pin hole. This method does not measure the thickness of the sample. However, with it is it possible to match the two surface topographies with each other.

8.3 Simulation results

In the material model used an elastic modulus is set to 36 GPa, a value that is roughly half of what is typically used for aluminium (68-72 GPa). The number originates from tensile tests performed on foil at Tetra Pak. The reason for being so low might be related to that thin foil only have a few grains in thickness. It might also be due to the thickness variation of the foil. Calculations made with the average macro thickness can give this number. If calculations were made locally at a point with low thickness the local area and global displacement would lead to a higher elastic modulus.

In the last simulations with the four node elements (C3D4) resulted in propagating necking in the MD model. Propagating necking is nothing you expect to see in a tensile test with metals. Plastic materials can show this behavior, since plastics is built up of long carbon chains. They can rearrange and stretch to form the propagating necking. Metals are only made up of single atoms formed in crystal lattice within grains. Atoms can only be rearranged and not be stretched. Therefore, there should not be propagating necking.

The final simulations resulted in a clear and concentrated localized neck. However, they showed some differences. The MD model neck was curvy. It might have followed a topographical valley on the matt side of the model. As seen in Figure 55 the failure of foil in a tensile test is not straight. This suggests that the simulation might be a realistic result.

Figure 55. Edge of the failure from a tensile test in MD direction. (Käck & Malmberg, 2015)

The neck in the 45° model was more of a straight line. It was perpendicular to the rolling lines and therefore in line with the valleys of the matt side. Other necks were also started to form in a zigzag pattern. The CD model had several necks, also formed in a zigzag pattern like those on the 45° model. The direction of the necks in the 45° and CD models are approximately 35 degrees from the horizontal axle. This angle is the same as when slip band forms in isotropic material. With an isotropic material model the necking is most possibly due to the formation of slip bands in the material and not to the topography.

The ratio visualized in Figure 53 is around 1:2.5. Figure 56 shows an image of a failure edge of aluminium foils from a tensile test taken in a SEM at Tetra Pak. The same ratio in this image is 1:2. If failure had been part of the model the same ratio might have been achieved. When failure occurs, the material regains its elastic deformation. That would make the length of the deformed edge shorter. This in turn would change the 1:2.5 ratio to a lower value, it might even become 1:2.

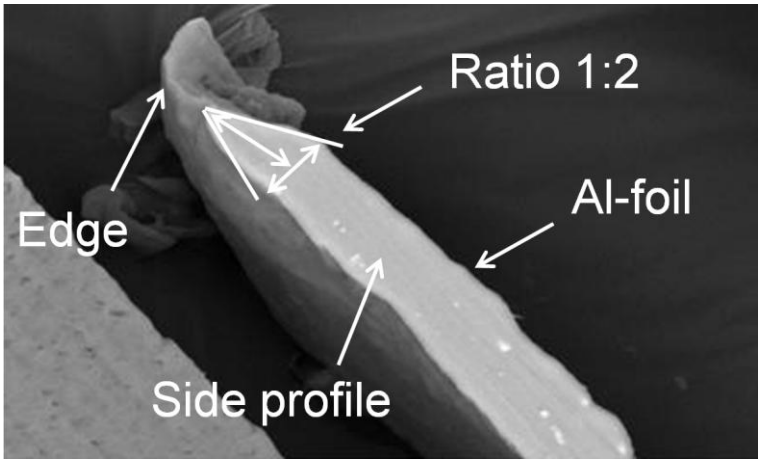

Figure 56. SEM image of a edge of failure from a tensile test. (Andeasson, Kao-Walter, & Ståhle, 2014)

The force displacement diagram in Figure 54 shows the result of the three simulations. Comparing those to the tensile tests performed by (Käck & Malmberg, 2015) some differences can be established. My material model was isotropic which resulted in the simulations all took roughly the same path until necking occurred. They found that tensile tests in 45 degrees could handle almost twice the amount of displacement. Of the three simulations in this thesis CD could cope with the most displacement and MD with the least. The reason for ABAQUS to abort the simulations is that the program could not find any more equilibrium for the models. Therefore, it can be said that the

topography is not the primary effect giving the results of the tensile test performed by Käck and Malmberg (Käck & Malmberg, 2015).

8.4 Work flow

Already from the beginning, a work flow was for planned the project. The work flow consists of five steps linked together in a way that has not been done before at Tetra Pak.

1. Find a suitable equipment for topography measurements
2. Perform the measurements, create a digital reconstruction of the foil surface
3. Use parameters and colour ranges to quantify and get a clear visualization of the surface topographies.
4. Transform the surface topographies into a mesh
5. Use the mesh in FEM-simulations

The work flow is visualized in Figure 57. This work flow could also be realized during the work with the thesis. The different steps have in this thesis been described in chronological order, with the exception of step four which is found in Appendix 0.

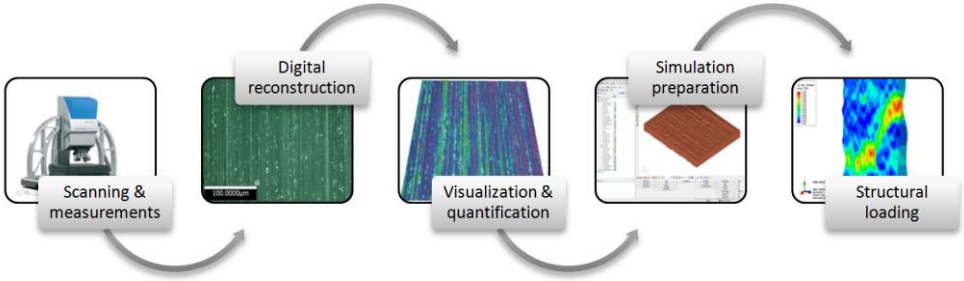

Figure 57. The work flow planned and used in this thesis.

9 Further work

This master thesis had focus on classifying the Al-foil and transfer the measurements into FEM simulations. Here come some examples of work that can be done as a continuation of this thesis.

- **Investigate other measurement methods**. The measurement method in this thesis did not generate a measurement of both sides in one measurement. The other methods in ISO 25 178-6 could be investigated along with some more powerful 3D-volume methods. Possibly looking into the possibility to use some instrument at ESS or MAX IV.
- **Validate the measurement results**. At the most was five measurements done on each side in this thesis. To get a statistical significance more measurements must be done. A thesis could concentrate on one of those comparisons I have done and get to decide the statistical significance. Especially interesting would it be to compare the contradictive results of the production with different worn work rollers, where the images and parameter values gave contradicting results.
- **Compare simulations with tensile test in SEM**. The SEM described in section 3.1.2.1 never got working during the time of this thesis. It will have a tensile stage making it possible to perform tensile tests in a SEM. That will give a possibility to validate the simulations made.
- **Continue with a more advanced simulation model**. This thesis made fairly simple simulations. Failure parameters were never successfully implemented. Investigations can be made with foils of different thicknesses or strengthen/weaken topography. I only used an isotropic material model. An anisotropic material model could be implemented or at least isotropic models for the specific tension directions of each model. If a measurement is done which capture the grains these can possibly also be implemented into a simulations. The surface topography can also be implemented into simulations of the whole packaging material.
- **Surface topographies impact on the adhesion**. An investigation can be how the different sides of the foil impact the adhesion. As shown in my work so are there some differences between the sides. How does the different surfaces on different foils impact on how the laminates react to the foil surface?

10 Bibliography

Alicona. (2016, 04 19). *InfiniteFocus.* Retrieved 04 19, 2016, from Direct Industry: http://pdf.directindustry.com/pdf/alicona-imaging/infinitefocus/20759-582043.html

Andeasson, E., Kao-Walter, S., & Ståhle, P. (2014). Micro-mechanisms of a laminated packaging material during fracture. *Engineering Fracture Mechanics 127* , 313-326.

Barten, A. (2002). *Aluminium Rolling Mill Technology: Future Concepts in Thin-strip and Foil Rolling.* Landsberg am Lech: Verlag Moderne Industrie.

Bengtsson, A., Börjesson, E., Carlsson, G., Ferrisius, J., Hedman, L., Johansson, F., et al. (2014). *CHARACTERIZATION OF THIN ALUMINIUMFOIL USED IN THE PACKAGING INDUSTRY.* Uppsala: Uppsala University.

Bruker AXS. (2006). *Introduction to x-ray flourecence (XRF)*. Retrieved 02 26, 2016, from https://web.archive.org/web/20080223224617/http:/www.bruker-axs.de/fileadmin/user_upload/xrfintro/sec1_3.html

Buffiere, J.-Y., Maire, E., Adrien, J., Masse, J.-P., & Boller, E. (2010). In Situ Experiments with X ray Tomography: An Attractive Tool for Experimental Mechanics. *Experimental Mechanics* (50), 289-305.

Callister Jr., W. D. (2001). *Fundamentals of Materials Science and Engineering* (First ed.). New York, NY: John Wiley & Sons, Inc.

Dhondt, G. (2014, 03 02). *Four-node tetrahedral element (C3D4 and F3D4)* . Retrieved 05 12, 2016, from Massachusets Institute of Technology: http://web.mit.edu/calculix_v2.7/CalculiX/ccx_2.7/doc/ccx/node32.html

European Aluminium Association, B., Støren, S., & Skanaluminium, O. (1994, 1 1). *TALAT Lecture 2101.01: Understanding Aluminium as a Material.* Retrieved 03 04, 2016, from CORE-Materials: http://core.materials.ac.uk/search/detail.php?id=2123

Käck, B., & Malmberg, C. (2015). *Aluminium foil at multiple length scales, mechanical tests and numerical simulations in Abaqus.* Lund: Division of Solid Mechanics, Lund University.

Maire, E., & Withers, P. J. (2013). Quantitative X-ray tomography. *International Materials Reviews , 59* (1), 1-43.

Michigan Metrology. (2016, April 27). *3D (areal) filtering, F-operator*. Retrieved April 27, 2016, from Michigan Metrology: http://www.michmet.com/3d_filtering_foperator.htm

Mishina, O. (2016, 05 03). Discussion about Aluminium alloys. (F. Larsson, Interviewer)

Mäkelä, P. (2012). An analytic procedure for determination of fracture toughness of paper materials. *Nordic Pulp and Paper Research Journal* , 352-360.

Reinhard Danzl, F. H. (2011). Focus Variation – a Robust Technology for High Resolution Optical 3D Surface Metrology. *Journal of Mechanical Engineering , 57* (3), 245-256.

SIS, Swedish Standards Institute. (2010). *SS-EN ISO 25178-6:2010.* Stockholm: SIS, Swedish Standards Institute.

The Aluminum Association, Inc. (2007). *Rolling Aluminum: From the Mine Through the Mill* (Third ed.). Arlington, VA: The Aluminum Association, Inc.

Woodward, R. (1994). *The Rolling of Aluminium: the Process and the Product.* Birmingham: European Aluminium Association.

A Surface measurement to FE-mesh

To be able to do simulations In ABAQUS the measurements needed to be transformed into a mesh. This appendix explains and shows how that transformation was done.

1. The measured surfaces can be exported to STL-files using the Alicona software. It is here possible to choose different grade of resolutions.
2. Two STL-files were imported to HyperMesh with ***Import Solver deck***, one file for the bright side and one for the matt side.
3. The bright side was moved using the command ***translate*** to position the surfaces on a correct distance from each other.
4. The matt side was rotated 180 degrees with the command ***rotate*** so the outside face of the surface would be oriented outward. Figure A1 shows the result after this step.

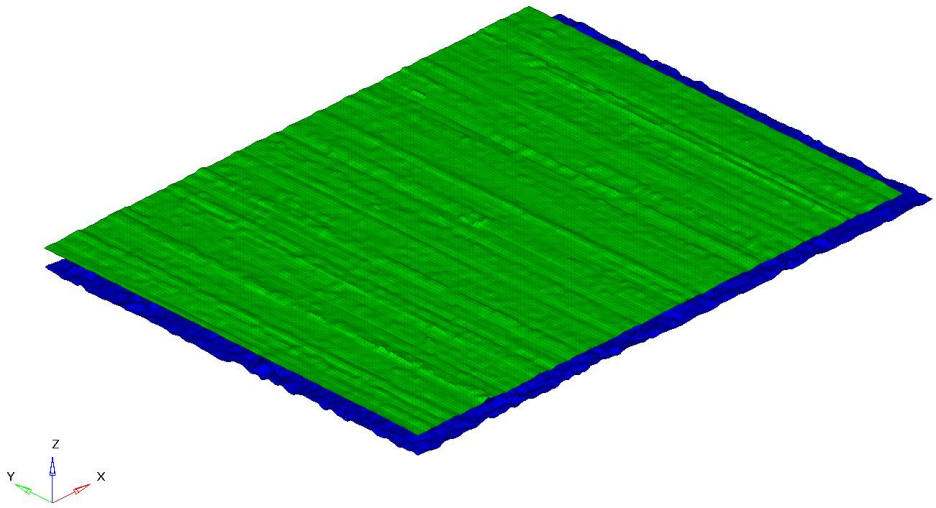

Figure A1. Two surfaces in HyperMesh after step 4.

5. The command ***organize*** was then used to crop both surfaces to the correct size. When selecting the size, awareness should be taken to computational time. Figure A2 shows how it looked like after this step.

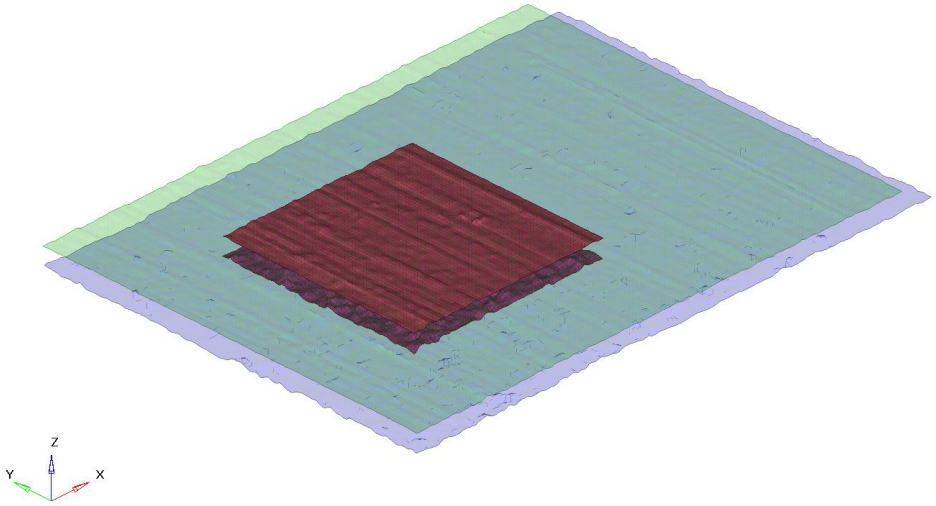

Figure A2. The measured data is cropped to the desired size.

6. To possibly add some extra elements to each surface and to connect the two surfaces with each other so an enclosure is created, the command ***ruled*** was used. Figure A3 shows the result after this step.

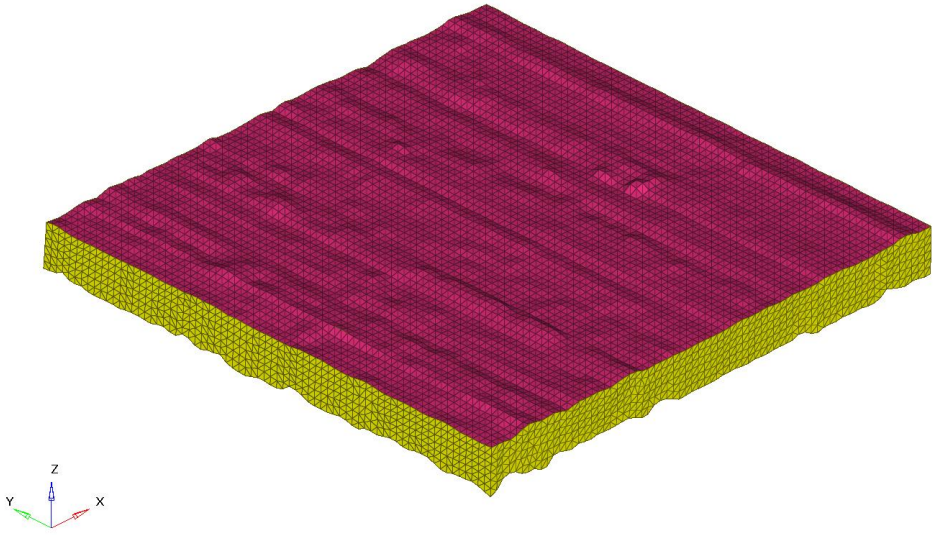

Figure A3. The cut from the surfaces together with the walls creating an enclosed volume.

7. When an enclosure is created by the surfaces and the newly added meshed walls the enclosure must be defined. This is made with the command ***edges***. This command glues together the different components and removes redundant nodes.

8. The command ***tetramesh*** *was used to fill the enclosure with tetrahedron shaped elements*. Figure A4 illustrates the mesh created in this step.

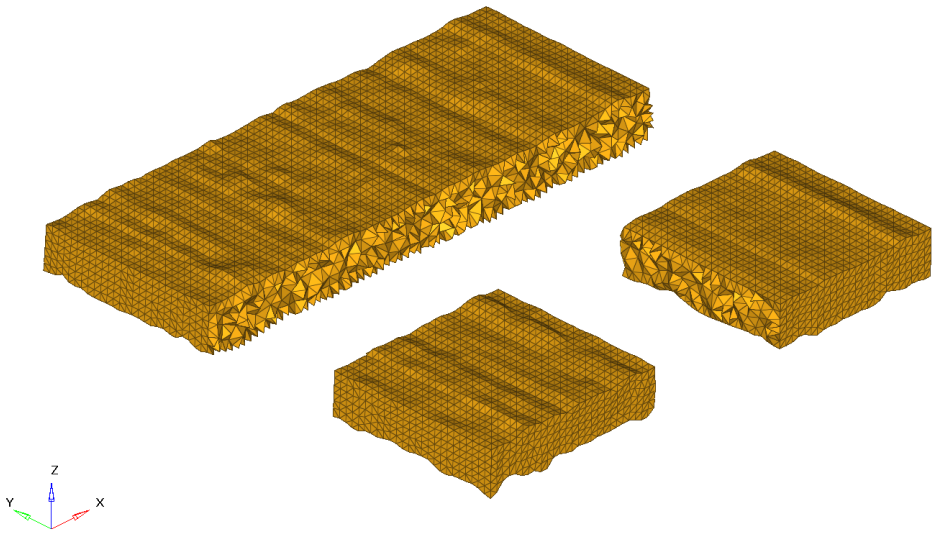

Figure A4. Cut-away view of the final mesh.

9. The finished mesh was then exported using ***Export Solver deck***.

The exported file can then be imported to ABAQUS or some other FE-analysis program for simulations.

The HyperMesh version used in this thesis was v14.0.

B Complementing result – Different sides of the foil

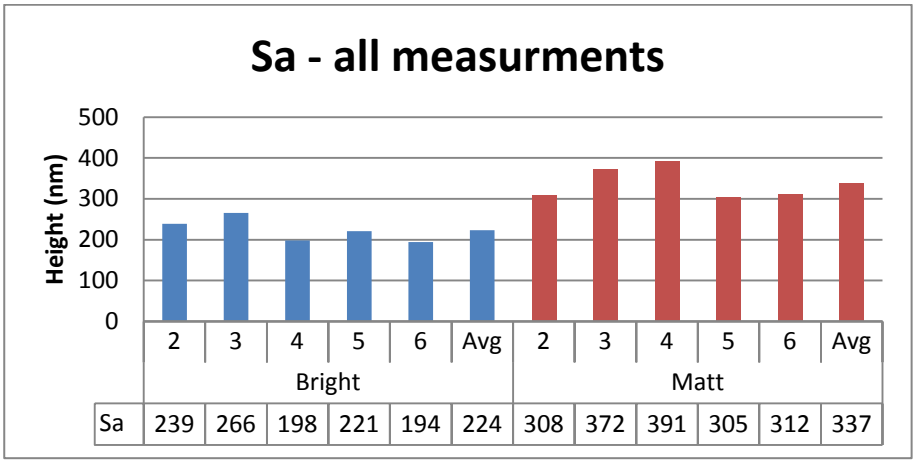

Figure B1. Measurement values of Sa and their average related to Figure 21.

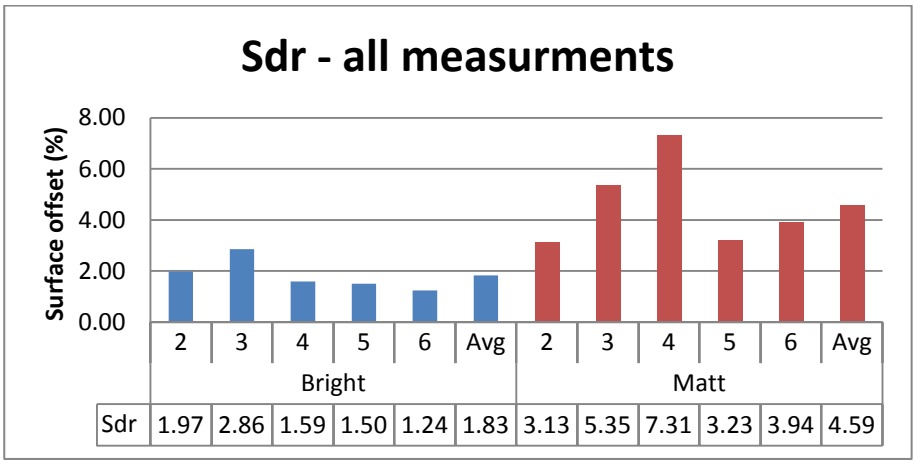

Figure B2. Measurement values of Sdr and their average related to Figure 22.

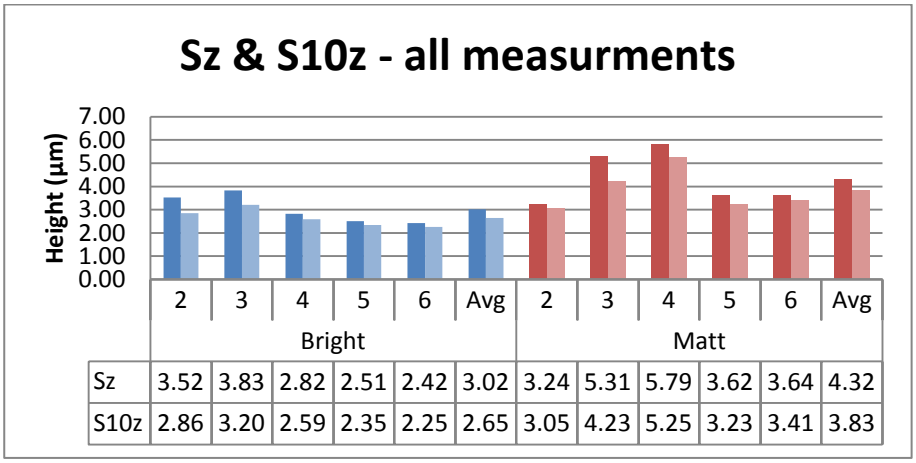

	2	3	4	5	6	Avg	2	3	4	5	6	Avg
Sz	3.52	3.83	2.82	2.51	2.42	3.02	3.24	5.31	5.79	3.62	3.64	4.32
S10z	2.86	3.20	2.59	2.35	2.25	2.65	3.05	4.23	5.25	3.23	3.41	3.83

Figure B3. Measurement values of Sz and S10z and thier averages related to Figure 23.

C Complementing results - Different wear on work rollers

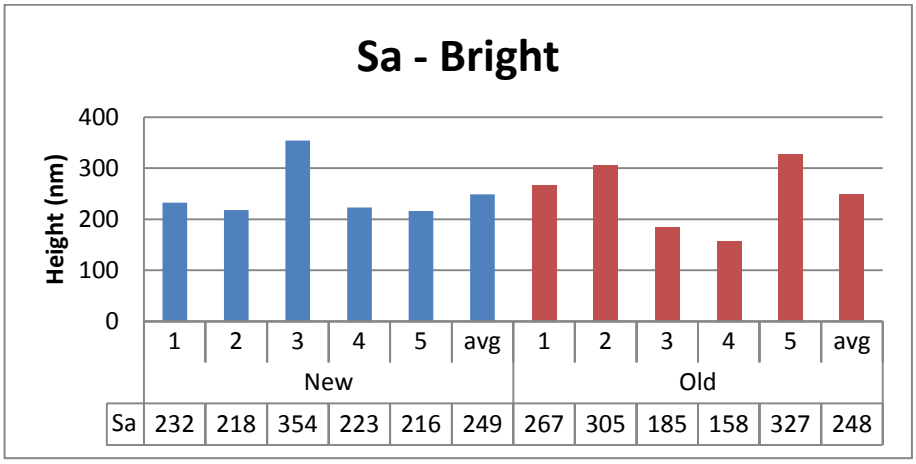

Figure C1. Measurement values of Sa on the bright side and their average related to Figure 36.

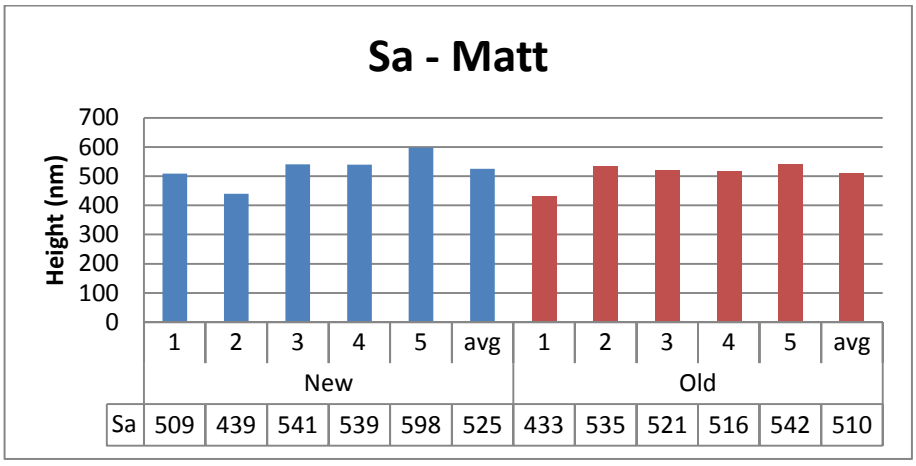

Figure C2. Measurement values of Sa on the matt side and their average related to Figure 36.

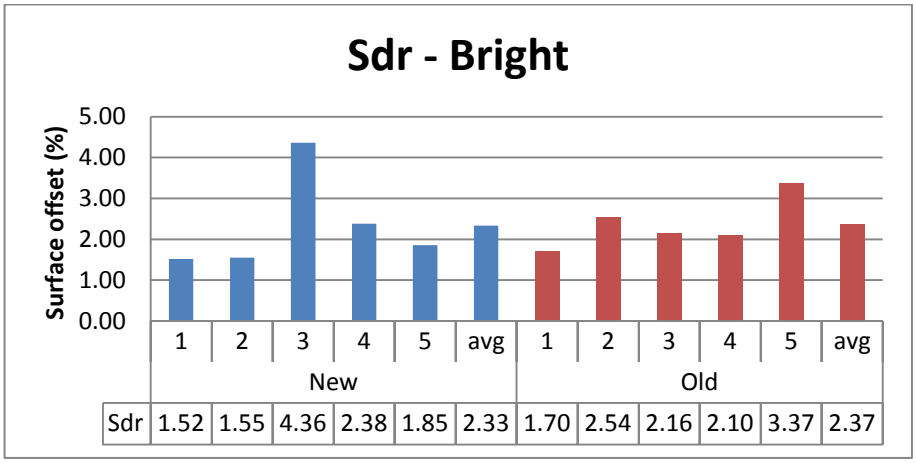

Figure C3. Measurement values of Sdr on the bright side and their average related to Figure 37

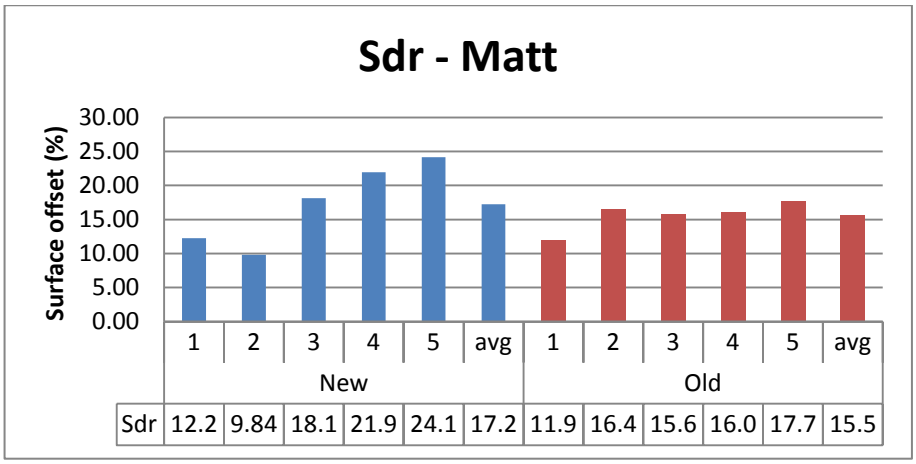

Figure C4. Measurement values of Sdr on the matt side and their average related to Figure 37.